



Iron from coal combustion particles dissolves much faster than mineral dust under simulated atmospheric acid conditions

Clarissa Baldo¹, Akinori Ito², Michael D. Krom^{3,4}, Weijun Li⁵, Tim Jones⁶, Nick Drake⁷, Konstantin Ignatyev⁸, Nicholas Davidson¹, Zongbo Shi¹

¹School of Geography Earth and Environmental Sciences, University of Birmingham, Birmingham, United Kingdom

²Yokohama Institute for Earth Sciences, JAMSTEC, Yokohama, Kanagawa 236-0001, Japan

³Morris Kahn Marine Station, Charney School of Marine Sciences, University of Haifa, Haifa, Israel

⁴School of Earth and Environment, University of Leeds, Leeds, United Kingdom

⁵Department of Atmospheric Sciences, School of Earth Sciences, Zhejiang University, Hangzhou 310027, China

⁶School of Earth and Environmental Sciences, Cardiff University, Cardiff, United Kingdom

⁷Department of Geography, King's College London, London, United Kingdom

⁸Diamond Light Source, Didcot, Oxfordshire, United Kingdom

Correspondence to: Zongbo Shi (z.shi@bham.ac.uk); Akinori Ito (akinori@jamstec.go.jp)

Abstract. Mineral dust is the largest source of total aerosol iron (Fe) loading over the offshore global ocean, but acidic processing of coal fly ash (CFA) in the atmosphere may result in a disproportionately higher contribution of bioavailable Fe. Here, we determined the Fe speciation and dissolution kinetics of CFA from Aberthaw (United Kingdom), Krakow (Poland), and Shandong (China) in solutions which simulate atmospheric acidic processing. In CFA-PM₁₀ fractions, 8%-21.5% of the total Fe was as hematite and goethite (dithionite extracted Fe), 2%-6.5 % as amorphous Fe (ascorbate extracted Fe), while magnetite (oxalate extracted Fe) varied from 3%-22%. The remaining 50%-87 % of Fe was associated with aluminosilicates. High concentration of ammonium sulphate ((NH₄)₂SO₄), often found in wet aerosols, increased Fe solubility of CFA up to 7 times at pH 2-3. Our

Deleted: to

Commented [MP1]: This hasn't been shown (to this extent) by any study. In order to have such impact CFA emissions would have to be both highly soluble (they are) and of very large magnitude (not shown to date). Maybe just pace own the sentence by choosing another word.

Commented [MP2]: Associated figure says "other" I cannot recall any data showing the remaining fraction is aluminosilicate. If no proof maybe correct to "remaining 50%-87 % of Fe was thought to be associated with ..." or "remaining 50%-87 % of Fe may be comprised in ..."

Deleted: low

Deleted: (

Deleted:)



results showed a large variability in the effects of oxalate on the Fe dissolution rates at pH 2, from no impact in Shandong ash to doubled dissolution in Krakow ash.

However, this enhancement was suppressed in the presence of high concentration of $(\text{NH}_4)_2\text{SO}_4$. Dissolution of highly reactive Fe was insufficient to explain the high Fe solubility at low pH in CFA, and the modelled dissolution kinetics suggests that other Fe phases such as magnetite may also dissolve rapidly under acidic conditions. Overall, Fe in CFA dissolved up to 7 times faster than in Saharan dust samples at pH 2. Based on these laboratory data, we developed a new scheme for the proton- and oxalate- promoted Fe dissolution of CFA, which was implemented into the global atmospheric chemical transport model IMPACT. The revised model showed a better agreement with observations of surface of dissolved Fe concentration in aerosol particles over the Bay of Bengal, due to the rapid Fe release at the initial stage at highly acidic conditions. The improved model also enabled us to predict sensitivity to a more dynamic range of pH changes, particularly between anthropogenic combustion and biomass burning aerosols.

1 Introduction

The availability of iron (Fe) limits primary productivity in high-nutrient low-chlorophyll (HNLC) regions of the global ocean including the subarctic North Pacific, the East Equatorial Pacific and the Southern Ocean (Boyd et al., 2007; Martin, 1990). In other regions of the global ocean such as the subtropical North Atlantic, the Fe input may affect primary productivity by stimulating nitrogen fixation (Mills et al., 2004; Moore et al., 2006). These areas are particularly sensitive to changes in the supply of bioavailable Fe. Atmospheric aerosols are an important source of soluble (and, thus potentially bioavailable) Fe to the offshore global ocean. The deposition of bioavailable Fe to the ocean can alter biogeochemical cycles and increase the carbon uptake, consequently affecting the climate (e.g., Jickells and Moore, 2015; Jickells et al., 2005; Kanakidou et al., 2018;

Commented [MP3]: Either because of the pH or because of differences in the samples...? I'd delete this sentence this is not the main finding

Commented [MP4]: No word on oxalate addition?

Commented [MP5]: Lybia (or just 'our reference dust sample')

Commented [MP6]: I do not think the model focuses on surface Fe dissolution only. Likely it accounts for Fe dissolution from one aerosol as a whole (although it is thought that surface Fe will dissolve first).

Formatted: Strikethrough

Formatted: Strikethrough

Deleted: concentration

Commented [MP7]: Community now tries to use "bioaccessible" Fe as the genuine bioavailability is still to prove.



64 Mahowald et al., 2010; Shi et al., 2012). In general, bioavailable Fe consists of
65 aerosol dissolved Fe, and Fe-nanoparticles which can be present in the original
66 particulate matter and/or formed during atmospheric transport as a result of cycling
67 into and out of clouds (Shi et al., 2009). It is in addition possible that other more
68 refractory forms of Fe could be solubilised in the surface waters by zooplankton
69 (Schlosser et al., 2018) or the microbial community (Rubin et al., 2011).
70 Atmospheric Fe is largely derived from lithogenic sources, which contribute around
71 95% of the total Fe in suspended particles (e.g., Myriokefalitakis et al., 2018) and
72 hence most studies concentrate on atmospheric processing of mineral dust (e.g.,
73 Cwiertny et al., 2008; Fu et al., 2010; Ito and Shi, 2016; Shi et al., 2011a; Shi et al.,
74 2015). Mineral dust has low Fe solubility (dissolved Fe/ total Fe) near the source
75 regions, generally below 0.5% (e.g., Schroth et al., 2009; Shi et al., 2011c),
76 increasing somewhat as a result of atmospheric processing (e.g., Baker et al., 2021;
77 Baker et al., 2020). Other sources of bioavailable Fe to the ocean are from
78 combustion sources such as biomass burning, coal combustion and oil combustion
79 (e.g., shipping emissions) (e.g., Ito et al., 2018; Rathod et al., 2020). Although these
80 sources are only a small fraction of the total Fe in atmospheric particulates, the Fe
81 solubility of pyrogenic sources can be 1–2 orders of magnitude higher than in
82 mineral dust, and thus can be important in promoting carbon uptake. However, the
83 Fe solubility of these sources vary considerably depending on the particular sources
84 with higher values observed for oil combustion and biomass burning (Ito et al.,
85 2021b and references therein).
86 Wang et al. (2015) estimated that coal combustion produces around $\sim 0.9 \text{ Tg yr}^{-1}$ of
87 atmospheric Fe (on average for 1960–2007), contributing up to $\sim 86\%$ of the total
88 anthropogenic Fe emissions. A more recent study, which has included metal

Commented [MP8]: Rephrase maybe 'most studies so far have concentrated on ...'

Commented [MP9]: I would say <1% is more accurate according to published literature

I'd suggest citing
Sholkovitz et al 2012
<http://dx.doi.org/10.1016/j.gca.2012.04.022>

Sholkovitz et al 2009
[10.1016/j.gca.2009.04.029](http://dx.doi.org/10.1016/j.gca.2009.04.029)

Commented [MP10]: Reference needed

Deleted: ,

Commented [MP11]: May be worth citing a lab-based or field-based study as well here.

Commented [MP12]: Emitted?

Commented [MP13]: Rephrase maybe '...of Fe into the atmosphere'



90 smelting as atmospheric Fe source, estimated that coal combustion emitted ~ 0.7 Tg
91 yr^{-1} of Fe for the year 2010, contributing around 34% of the total anthropogenic Fe
92 (Rathod et al., 2020). Although the use of coal as a principle energy source has been
93 recently reduced as a result of concern about air quality and global warming, coal is
94 still an important energy source in a number of countries in particular in the Asia-
95 Pacific region (BP, 2020). In China, most of the total energy is supplied by coal,
96 contributing over 50% of the global coal consumption in 2019, followed by India
97 (12%), and the US (8%). Germany and Poland are the largest coal consumers in
98 Europe, accounting together for around 40% of the European usage (BP, 2020).
99 South Africa is also among the principal countries for coal consumption (BP, 2020)
100 and is a source of particles to the Fe-limited Southern Ocean (e.g., Ito et al., 2019).
101 Coal fly ash (CFA) is a by-product of coal combustion. This generally consists of
102 glassy spherical particles (e.g., Brown et al., 2011), which are formed through
103 different transformations (decomposition, fusion, agglomeration, volatilization) of
104 mineral matter in coal during combustion (e.g., Jones, 1995), and are transported
105 with the flue gases undergoing rapid solidification. CFA are co-emitted with acidic
106 gases such as sulphur dioxide (SO_2), nitrogen oxides (NO_x) and carbon dioxide
107 (CO_2) (e.g., Munawar, 2018).
108 During long-range transport, CFA particles undergo atmospheric processing with
109 the CFA surface coated by acidic species such as sulphuric acid (H_2SO_4) and oxalic
110 acid ($\text{H}_2\text{C}_2\text{O}_4$) in atmospheric aerosols. Aged CFA particles are hygroscopic and
111 absorb water at typical relative humidity in the marine atmosphere, which forms a
112 thin layer of water with high acidity, low pH and high ionic strength (Meskhidze et
113 al., 2003; Spokes and Jickells, 1995; Zhu et al., 1992). In addition, ammonia (NH_3)
114 which is a highly hydrophilic gas, can also partition into the aerosol phase, react
115 with H_2SO_4 and form ammonium sulphate ($(\text{NH}_4)_2\text{SO}_4$) an important inorganic salt
116 contributing to the high ionic strength in such atmospheric aerosols (Seinfeld and
117 Pandis, 2016).

Commented [MP14]: Rephrase maybe '...of the total anthropogenic Fe atmospheric loading'

Commented [MP15]: Rephrase maybe '... is a source of Fe-bearing particles to the anemic Southern Ocean'

Deleted: .

Deleted: This

Commented [MP16]: ... around the particle

Commented [MP17]: Are you referring to CFA here?



120 At low pH conditions, Fe solubility in aerosols increases, as the high concentration
121 of protons (H^+) weakens the Fe-O bonds facilitating the detachment of Fe from the
122 surface lattice (Furrer and Stumm, 1986). Li et al. (2017) provided the first
123 observational evidence that acidification leads to the release of Fe from
124 anthropogenic particles.

125 In addition to these inorganic processes, organic ligands can also enhance
126 atmospheric Fe dissolution by forming soluble complexes with Fe (e.g., Cornell and
127 Schwertmann, 2003). For example, $H_2C_2O_4$ is an important organic species in
128 aerosols (e.g., Kawamura and Bikkina, 2016). Laboratory studies have
129 demonstrated that $H_2C_2O_4$ increases Fe solubility of aerosol sources (Chen and
130 Grassian, 2013; Paris and Desboeufs, 2013; Paris et al., 2011; Xu and Gao, 2008).
131 Recently, observations over the Bay of Bengal indicate that $H_2C_2O_4$ contributes to
132 the increase in water dissolvable, atmospheric Fe (Bikkina et al., 2020).

133 To simulate the Fe dissolution in CFA, it is necessary to determine the dissolution
134 kinetics under realistic conditions. Previous studies have investigated the Fe
135 dissolution kinetics of CFA under acidic conditions. Chen et al. (2012) simulated
136 acidic and cloud processing of certified CFA. Fu et al. (2012) determined the
137 dissolution kinetics of CFA samples at pH 2, while Chen and Grassian (2013)
138 investigated the effect of organic species (e.g., oxalate and acetate) at pH 2-3. These
139 studies showed that high acidity and the presence of oxalate enhanced Fe
140 dissolution, similar to those reported in mineral dust (Chen et al., 2012; Chen and
141 Grassian, 2013; Fu et al., 2012; Ito and Shi, 2016; Shi et al., 2011a). They also
142 demonstrated that there are large differences in dissolution rates in different types of
143 CFA, likely related to Fe speciation.

Deleted: to confirm

Deleted: the

Commented [MP18]: Oxalic acid? Maybe spell out the name when first encountered

Deleted: atmospheric

Commented [MP19]: Atmospheric aerosol seems redundant

Deleted: atmospheric

Deleted: atmospheric

Deleted: ed

Commented [MP20]: '... at the surface of CFA particles'



150 Furthermore, high ionic strength, commonly seen in aerosol water, affects the
151 activity of molecular species present in solution, consequently it can significantly
152 impact the Fe dissolution behaviour. Recent studies have considered the effect of
153 the high ionic strength on the Fe dissolution kinetic of CFA under acidic conditions.
154 For example, the Fe solubility of CFA samples was measured at pH 1-2 with high
155 sodium chloride (NaCl) concentrations (Borgatta et al., 2016), and with high
156 sodium nitrate (NaNO₃) concentrations Kim et al. (2020). In real atmospheric
157 conditions, NaCl or NaNO₃ are unlikely to be the main driver of high ionic strength
158 in aged CFA. Although NaCl can coagulate with dust particles in the marine
159 boundary layer (Zhang et al., 2003), the aging of coal fly ash is primarily by the
160 uptake of secondary species, particularly sulphate and ammonia (Li et al., 2003). Ito
161 and Shi (2016) found that, at low pH and high concentration of (NH₄)₂SO₄, the Fe
162 solubility of mineral dust is likely to be enhanced by the adsorption of sulphate ions
163 on the particle surface. However, to date the effect of high (NH₄)₂SO₄
164 concentrations on the Fe dissolution behaviour in combustion sources in the
165 presence or absence of oxalate remains unknown.
166 The dissolution kinetics measured by Chen and Grassian (2013) has been used to
167 develop a modelled dissolution scheme for CFA, assuming a single Fe phase in
168 CFA (Ito, 2015). However, there are multiple Fe phases in CFA, primarily hematite,
169 magnetite and ~~Fe in~~ aluminium silicate glass (Brown et al., 2011; Chen et al., 2012;
170 Fu et al., 2012; Kukier et al., 2003; Kutchko and Kim, 2006; Lawson et al., 2020;
171 Sutton, 2018; Valeev et al., 2019; Waanders et al., 2003; Wang, 2014; Zhao et al.,
172 2006), but also accessory Fe-bearing minerals for example silicates, carbonate,
173 sulphides and sulphates (Zhao et al., 2006). These phases have a range of
174 reactivities. Previous studies showed that CFA dissolves much faster during the first
175 1-2 hours than subsequently (Borgatta et al., 2016; Chen et al., 2012; Chen and
176 Grassian, 2013; Fu et al., 2012; Kim et al., 2020), confirming the large difference in
177 Fe dissolution from different phases.

Commented [MP21]: kinetics

Commented [MP22]: called 'CFA' up to then

Deleted:

Commented [MP23]: Is the term 'phase' commonly used to refer to the mineralogy of the particles holding Fe?

Formatted: Strikethrough

Commented [MP24]: I would pace that down. 'confirming the existence of different Fe-bearing mineral 'phases' within a single CFA sample.



179 In this study, laboratory experiments were conducted to determine the dissolution
180 kinetics of coal combustion **sources** (e.g., **coal fly ash**) during simulated
181 atmospheric acidic processing in the presence of $(\text{NH}_4)_2\text{SO}_4$ and oxalate which are
182 commonly found in atmospheric aerosols. In particular, we investigated the effect of
183 high $(\text{NH}_4)_2\text{SO}_4$ concentrations on the protonpromoted and oxalate-promoted Fe
184 dissolution at low pH conditions. Our study also determined the Fe phases present
185 in the CFA and compared them to those present in mineral dust. The experimental
186 results enabled us to develop a new Fe release scheme for CFA sources which was
187 then implemented into the global atmospheric chemical transport model IMPACT.
188 The model results were compared with observations of surface concentration of
189 dissolved Fe in aerosol particles over the Bay of Bengal from Bikkina et al. (2020).

190 2 Materials and Methods

191 2.1 Sample collection and subsequent size fractionation

192 CFA samples were collected from the electrostatic precipitators at three coal-fired
193 power stations at different locations: United Kingdom (Aberthaw ash), Poland
194 (Krakow ash), and China (Shandong ash). The bulk samples were resuspended to
195 obtain **dust fractions** representative of particles emitted into the atmosphere. A
196 custom-made resuspension system was used to collect the PM_{10} fraction (particles
197 with an aerodynamic diameter smaller than $10\ \mu\text{m}$), which is shown in Fig. S1.
198 Around 20 g of sample was placed into a glass bottle and injected at regular
199 intervals (2-5 sec) into a glass reactor ($\sim 70\ \text{L}$) by flushing the bottle with pure
200 nitrogen. The air in the reactor was pumped at a flow rate of $30\ \text{L min}^{-1}$ into a PM_{10}
201 sampling head. Particles were collected on $0.6\ \mu\text{m}$ polycarbonate filters and
202 transferred into centrifuge tubes. The system was cleaned manually and flushed for

Commented [MP25]: Samples?

Commented [MP26]: called 'CFA' up to then

Commented [MP27]: I am wondering about the use of the word "dust" sometimes in the manuscript. "Dust" would refer to a lithogenic mineral source (wind-blown soil). Maybe dust here would rather be changed to "aerosol fractions" which is the generic term for 'particulates suspended in the air'



10 min with pure nitrogen before loading a new sample. A soil sample from Libya (Soil 5, 32.29237N/22.30437E) was dry sieved to 63 μm (which is referred to as Libya dust) and used for the comparison of CFA with mineral dust.

2.2 Fe dissolution kinetics

The Fe dissolution kinetics of the CFA samples was determined by time-dependent leaching experiments. We followed a similar methodology as in Ito and Shi (2016). PM_{10} fractions were exposed to H_2SO_4 solutions at pH 1, 2 or 3, in the presence of $\text{H}_2\text{C}_2\text{O}_4$ and/or $(\text{NH}_4)_2\text{SO}_4$ to simulate acidic processing in aerosol conditions. The concentration of $\text{H}_2\text{C}_2\text{O}_4$ in the experiment solutions was chosen based on the molar ratio of oxalate and sulphate in $\text{PM}_{2.5}$ (particles with an aerodynamic diameter smaller than 2.5 μm) from observations over the East Asia region (Yu et al., 2005). Around 50 mg of CFA was leached in 50 ml of acidic solution to obtain a dust/liquid ratio of 1 g L^{-1} . The sample solution was mixed continuously on a rotary mixer, in the dark at room temperature. A volume of 0.5 mL was sampled at fixed time intervals (2.5, 15, 60 min and 2, 6, 24, 48, 72, and 168 hours after the CFA sample was added to the experiment solution) and filtered through 0.2 μm pore size syringe filters. The dissolved Fe concentration in the filtrate was determined using the ferrozine method (Viollier et al., 2000). Leaching experiments were also conducted on the Libya dust. The relative standard deviation (RSD) at each sampling time varied from 4 % to 15 % ($n=7$).

The pH of all the experiment solutions was calculated using the E-AIM model III for aqueous solutions (Wexler and Clegg, 2002). In part this was because the high ionic strength generated by the elevated concentration of $(\text{NH}_4)_2\text{SO}_4$ prevents electrochemical sensors from making accurate pH measurements. For the experiment solutions with no $(\text{NH}_4)_2\text{SO}_4$, the pH was measured by a pH meter before adding the ash and at the end of the experiments. The solution pH increased after adding the ash, and the change in pH was used to estimate the buffer capacity of alkaline minerals in the samples, including for example calcium carbonates

Commented [MP28]: Change to "aerosols"



(CaCO₃), lime (CaO), and portlandite (Ca(OH)₂). The estimated concentration of H⁺ buffered was used to input the concentration of H⁺ into the E-AIM model. For each experiment, the pH was calculated before adding the CFA samples and at the end of the experiments. The pH of the original solution before adding the samples was estimated from the molar concentrations (mol L⁻¹) of H₂SO₄, H₂C₂O₄ and (NH₄)₂SO₄ used to prepare the solution. The model inputs included the total concentrations of H⁺ (without H₂C₂O₄ contribution), NH₄⁺, SO₄²⁻ and H₂C₂O₄. For the experiment solutions with no (NH₄)₂SO₄, we calculated the final pH by reducing the total H⁺ concentration input into the model to match the pH measured at the end of the experiments. The buffered H⁺ was then estimated from the difference between the original and final H⁺ concentration input into the model. To determine the final pH of the solutions with high ionic strength, the H⁺ concentration input in the model was calculated as the difference between the H⁺ concentration in the original solution and the buffered H⁺ estimated at low ionic strength. For the solution with no (NH₄)₂SO₄, the difference between calculated and measured pH is <7%. Table S1 reports the concentrations of H₂SO₄, H₂C₂O₄ and (NH₄)₂SO₄ in the experiment solutions, the original and final pH from model estimates (including H⁺ concentrations and activities), and the pH measurements for the solution with low ionic strength.

2.3 Sequential extractions

The content of Fe oxide species in the samples was determined by Fe sequential extraction (Baldo et al., 2020; Poulton and Canfield, 2005; Raiswell et al., 2008; Shi et al., 2011b). The Fe oxide species included highly reactive amorphous Fe oxidehydroxide (FeA), crystalline Fe oxide-hydroxide, mainly goethite and hematite (FeD), and Fe associated with magnetite (FeM).



To extract FeA, samples were leached in an ascorbate solution buffered at pH 7.5 (Raiswell et al., 2008; Shi et al., 2011b). The ascorbate solution contained a deoxygenated solution of 50 g L⁻¹ sodium citrate, 50 g L⁻¹ sodium bicarbonate, and 10 g L⁻¹ of ascorbic acid. Around 30 mg of CFA was leached for 24 hours in 10 mL of ascorbate extractant, mixed continuously on a rotary mixer. The extraction solution was then filtered through a 0.2 µm membrane filter. In order to extract FeD, the residue was leached for 2 more hours in a dithionite solution buffered at pH 4.8 (50 g L⁻¹ sodium dithionite in 0.35 M acetic acid and 0.2 M sodium citrate) (Raiswell et al., 2008; Shi et al., 2011b).

For the extraction of FeM, the CFA samples were first leached for 2 hours using a citrate-buffered dithionite solution to remove FeD. The residue collected after filtration was then leached for 6 hours in a solution of 0.2 M ammonium oxalate ((NH₄)₂C₂O₄) and 0.17 M H₂C₂O₄ at pH 3.2 (Poulton and Canfield, 2005). The Fe extractions were all carried out in the dark at room temperature. The Fe concentration in the filtered extraction solutions was measured using the ferrozine method (Viollier et al., 2000) or by inductively coupled plasma optical emission spectrometry (ICP-OES) analysis for the solutions containing high concentration of oxalate.

The total Fe content in the samples was determined by microwave digestion in concentrated nitric acid (HNO₃) followed by inductively coupled plasma mass spectrometry (ICP-MS) analysis.

The RSD% obtained for each extract using the Arizona test dust was 3% for FeA, 11% for FeD, 12% for FeM and 2% for the total Fe (n=7).

2.4 X-ray absorption near edge structure (XANES) analysis

We collected XANES spectra to qualitatively examine the Fe speciation in the CFA samples. The XANES spectra at the Fe K-edge were collected at the Diamond Light Source beamline I18. A Si(111) double-crystal monochromator was used in the experiments. The beam size was 400 µm×400 µm. The XANES spectra were

Commented [MP29]: No HF used for digestion? Did you check the recovery, especially for the dust material (Libya dust and ATD)?

Commented [MP30]: What values do you use for reference? (REF?)



collected from 7000 to 7300 eV at a resolution varying from 0.2 eV for 3 s in proximity to the Fe K-edge (7100–7125 eV) to 5 eV for 1 s from 7100 to 7300 eV. Powder samples were suspended in methanol and deposited on Kapton® tape. The analysis was repeated three times. We measured the XANES spectra of the CFA-PM₁₀ fractions and mineral standards including hematite, magnetite, and illite. Data were processed using the Athena program, part of the software package Demeter (version 0.9.26) (Ravel and Newville, 2005).

2.5 Model description

This study used the Integrated Massively Parallel Atmospheric Chemical Transport (IMPACT) model (Ito et al., 2021a and references therein). The model simulates the emission, chemistry, transport, and deposition of Fe-containing aerosols and the precursor gases of inorganic and organic acids. The coating of acidic species on the surface of Fe-containing aerosols promotes the release of soluble Fe in the aerosol deliquescent layer and enhances the aerosol Fe solubility (Li et al., 2017). On the other hand, the external mixing of oxalate-rich aerosols with Fe-rich aerosols can suppress the oxalate-promoted Fe dissolution at low concentration of oxalate near the source regions (Ito, 2015). However, the internal mixing of alkaline minerals such as calcium carbonate with Fe-containing dust aerosols can suppress the Fe dissolution (Ito and Feng, 2010). Since CFA particles are co-emitted with acidic species, the transformation of relatively insoluble Fe in coal combustion aerosols into dissolved Fe is generally much faster than that for mineral dust aerosols during their atmospheric lifetime (Ito, 2015; Ito and Shi, 2016). Additionally, the size of CFA particles is substantially smaller than that of mineral dust. Thus, we adopted an observationally constrained parameter for the dry deposition scheme (Emerson et al., 2020) to improve the simulation of dry deposition velocity of fine particles.



To improve the accuracy of our simulations of Fe-containing aerosols, we revised the on-line Fe dissolution schemes in the original model (Ito et al., 2021a) in conjunction with the mineralogy-based emission rates and a more dynamic range of pH estimates. To implement 3-step dissolution schemes, we used the mineral-specific emission inventory for anthropogenic Fe emissions (Rathod et al., 2020). To apply the Fe dissolution schemes for high ionic strength in aerosols, we used the mean activity coefficient for pH estimate (Pye et al., 2020). Moreover, the dissolution rate was assumed to be dependent of pH for highly acidic solutions (pH < 2) unlike in the former dissolution scheme (Ito, 2015), which allowed us to predict the sensitivity of Fe dissolution to pH lower than 2.

To validate the new dissolution scheme, we compared our model results with observations of surface concentration of dissolved Fe in PM_{2.5} aerosol particles over the Bay of Bengal (Bikkina et al., 2020).

3 Experimental results

3.1 Fe dissolution kinetics

We determined that Krakow ash had the largest buffer capacity, around 0.008 moles of buffered H⁺ per litre, which was related to the content of alkaline minerals in the sample. The buffer capacity of Aberthaw and Shandong ash was ~10 times smaller than that of Krakow ash, around 0.0007 moles of buffered H⁺ per litre. Leaching Krakow ash in 0.005 M H₂SO₄, the initial concentration of H⁺ was similar to the concentration of the H⁺ buffered. As a result, the solution pH raised from approximately 2.1 to 2.7 corresponding to a pH change of around 20% (Table S1). For all the other experimental conditions, the pH change was below 12% (Table S1). At the pH conditions used in this study (pH 1-3), acid buffering was fast and likely occurred within the first 1-2 hours. We assumed that the calculated final pH was representative of the solution pH over the duration of the experiments.



Dissolved Fe at different time intervals is reported as Fe%, which is the fraction of Fe dissolved to the total Fe content (FeT) in the CFA samples. For all samples, a fast dissolution rate was observed at the beginning of the experiment. In the case of Krakow ash, a dissolution plateau was reached after 2-hour leaching, which was likely due to the pH change. For that sample/initial condition the pH increased to 2.7, and no more Fe was dissolved, leading to a total Fe solubility of ~9% over the duration of the experiment (7 days) (Fig. 1a). Dissolving Krakow ash in 0.01 M H₂SO₄ (Fig. 1a), the experiment solution had a final calculated pH of 2.1. The total Fe solubility was 34% at pH 2.1, almost 4 times higher than that at pH 2.7 (in 0.005 M H₂SO₄). Dissolution of Aberthaw and Shandong ash was slower compared to Krakow ash (Figs. 1b and 2c, respectively).

Leaching Aberthaw and Shandong ash in 0.005 M H₂SO₄ resulted in solutions with a pH of around 2.2. At this pH, the total Fe solubility was 18% for Aberthaw ash and 21% for Shandong ash, which is 9-10 times higher than the total Fe solubility at pH 2.9 (in 0.001 M H₂SO₄), around 2% for both samples.

The experimental treatment of dissolved Fe from Krakow ash in 0.05 H₂SO₄ solution with 1 M (NH₄)₂SO₄ (Fig. 1a) resulted in a final predicted pH of 2.1. At that pH, the total Fe solubility of Krakow ash increased from 34% with no (NH₄)₂SO₄ to 48% with high (NH₄)₂SO₄ concentration. The total Fe solubility of Krakow ash was around 28% at pH 3.0 with 1 M (NH₄)₂SO₄ (Fig. 1a), 3 times higher than that at pH 2.7 with no (NH₄)₂SO₄. At around pH 2, the total Fe solubility of Aberthaw (Fig. 1b) and Shandong ash (Fig. 1c) increased by around 20% and 30% in the presence of (NH₄)₂SO₄. By contrast, the total Fe solubility at pH 3.1 with 1 M (NH₄)₂SO₄ was 7.5% for Aberthaw ash (Fig. 1b) and 14% for

Commented [MP31]: May I suggest a summary table in the manuscript reporting each pH, H₂SO₄ concentration, addition of H₂C₂O₄ and NH₄SO₄ would make the reading much easier.



Shandong ash (Fig. 1c), respectively, which was around 4 and 7 times higher than in the experiments carried out at pH 2.9 without $(\text{NH}_4)_2\text{SO}_4$.

The Fe dissolution of the CFA samples in H_2SO_4 solutions with 0.01 M $\text{H}_2\text{C}_2\text{O}_4$ (at around pH 2) is shown in Fig. 2. The total Fe solubility of Krakow ash at pH 1.9 with 0.01 M $\text{H}_2\text{C}_2\text{O}_4$ was 61% (Fig. 2a), which was almost 2 times higher than that at pH 2.1 but without $\text{H}_2\text{C}_2\text{O}_4$ (Fig. 2a). For Aberthaw ash, oxalate contribution to the dissolution process led to a total Fe solubility of 30% at pH 2.0 (Fig. 2b), which was 70% higher than in the experiment carried out in 0.005 M H_2SO_4 (~pH 2.2) (Fig. 2b). Shandong ash dissolution behaviour was not affected by the presence of oxalate (Fig. 2c).

We also investigated the effect of high $(\text{NH}_4)_2\text{SO}_4$ concentration on oxalate-promoted dissolution. In Fig. 2a, the total Fe solubility of Krakow ash decreased from 61% at pH 1.9 in the presence of oxalate to 54% at pH 2.0 with oxalate and $(\text{NH}_4)_2\text{SO}_4$. For Aberthaw ash, the total Fe solubility at pH 2.0 decreased from 30% in the presence of oxalate to 19% after the addition of $(\text{NH}_4)_2\text{SO}_4$ (Fig. 2b).

Figure 3 shows the Fe dissolution behaviour of Krakow ash at different pH conditions in the presence of 1 M $(\text{NH}_4)_2\text{SO}_4$ and $\text{H}_2\text{C}_2\text{O}_4$ (0.01-0.03 M depending on the solution pH). The total concentration of oxalate ions was calculated using the E-AIM model and was similar at different pH conditions, 0.015 at pH 1.0 (Experiment 7 Table S2), 0.009 at pH 2.0, and 0.01 at pH 2.9 (Experiments 3 Table S2). The highest total Fe solubility was observed at pH 1.0 (~67%). At pH 2.0, the total Fe solubility decreased to 54%, and no substantial variations were observed between pH 2.0 and pH 2.9 (54%-51%). At pH 1.0, the concentration of H^+ was considerably higher compared to pH 2.0-2.9, leading to a faster dissolution rate. The total concentration of oxalate ions was 1.5-1.6 times higher in the solution at pH 1.0 than at pH 2.0-2.9, which may also contribute to the faster dissolution rate. $\text{C}_2\text{O}_4^{2-}$ concentration increased with rising pH. Although the concentration of H^+ was lower



at pH 2.9 than at pH 2.0, the E-AIM model estimated that $\text{C}_2\text{O}_4^{2-}$ contributed around 35% of the total oxalate concentration at pH 2.9, which was 4.5 times higher than at pH 2.0 (Experiments 3 Table S2). The similar dissolution behaviour at pH 2.0 and pH 2.9 conditions may reflect the combination of these two opposite factors, higher concentration of $\text{C}_2\text{O}_4^{2-}$ but lower concentration of H^+ at pH 2.9 compared to 2.0.

We determined the Fe dissolution behaviour of Krakow ash at pH 1.0 in the presence of oxalate and increasing concentrations of $(\text{NH}_4)_2\text{SO}_4$. The ash was leached in H_2SO_4 solutions with 0.03 M $\text{H}_2\text{C}_2\text{O}_4$ at pH 1.0, while the concentration of $(\text{NH}_4)_2\text{SO}_4$ varied from 0 to 1.5 M. In Fig. 4, the total Fe solubility of Krakow ash in the presence of oxalate was 75% at pH 1.0 and decreased to 68% after the addition of 0.5 M $(\text{NH}_4)_2\text{SO}_4$. Higher $(\text{NH}_4)_2\text{SO}_4$ concentrations did not affect the Fe dissolution behaviour in the presence of oxalate at pH 1.0.

3.2 Fe speciation

The Fe phases in the CFA samples determined through sequential extractions are shown in Fig. 5. The Fe speciation in the Saharan dust sample is added for comparison. Krakow ash had a total Fe (FeT) content of 5.2%, while FeT in Aberthaw and Shandong ash was 3.1% and 1.6% respectively. Amorphous Fe (FeA/FeT) was 6.5% in Krakow ash, 2% in Aberthaw ash, and 4.6% in Shandong ash. The CFA samples showed very different dithionite Fe (FeD/FeT) content, 21.5% in Krakow ash, 8% in Aberthaw ash and 14.8% in Shandong ash. The content of magnetite (FeM/FeT) was considerably higher in Krakow ash (22.4%) compared to Aberthaw (2.9%) and Shandong (4.5%) ash. About 50 %–87 % of Fe was contained in other phases most likely in aluminosilicates. Overall, CFA had

Commented [MP32]: On Fig 4 it looks like the addition of $(\text{NH}_4)_2\text{SO}_4$ does slightly (yet noticeably) diminish the Fe dissolution. Or is that another factor coming into play?

Commented [MP33]: If this is the Libya dust, please keep the name consistent throughout



more magnetite and highly reactive amorphous Fe and less dithionite Fe than Libya dust.

In Fig. S2, the Fe K-edge XANES spectra of Krakow and Aberthaw ash showed a single peak in the pre-edge region at around 7114.3 eV and 7114.6 eV, respectively. In the edge region, Aberthaw ash showed a broad peak at around 7132.2 eV, while the peak of Krakow ash was slightly shifted to 7132.9 eV and narrower. The pre-edge peak at around 7115.4 suggest that Fe was mainly as Fe(III). The spectral features of Aberthaw and Krakow ash are different from those of the hematite, magnetite and illite standards suggesting that the glass fraction was dominant and controlled their spectral characteristics, which is consistent with the results of the Fe sequential extractions. The XANES Fe K-edge spectra of the CFA samples have some common features with those of Icelandic dust, but differs from northern African dust (Fig. S2). Aluminium silicate glass is also dominant in Icelandic dust (Baldo et al., 2020). In the pre-edge region, Icelandic dust (sample MIR 45 in Fig. S2) showed a main peak at around 7114.4 eV and a second less intense peak at around 7112.7 eV, while a broad peak was observed at around 7131.9 eV in the edge region (Baldo et al., 2020). Northern African dust (western Sahara in Fig. S2) showed a distinct double peak in the pre-edge region at around 7113.9 and 7115.2 eV, and a main peak in the edge region at around 7133.3 eV (Baldo et al., 2020).

4 Fe simulation from the IMPACT model

4.1 Fe dissolution scheme

Based on the laboratory experiments carried out on the CFA samples, we implemented a 3-step dissolution scheme for protonpromoted and oxalate-promoted Fe dissolution (Table 1). The Fe dissolution kinetics was described as follows (Ito, 2015):

Commented [MP34]: Please develop slightly the reasoning here

Commented [MP35]: This is a funny parallel between CFA and dust, why would similarities be expected? Is that in order to better understand the composition (mineralogy) of the CFA? Is the exact composition of the Icelandic dust known? Is it dust or aerosols collected at a random location in Iceland? Maybe a word to understand why the parallel between CFA and dust is made would help.

Commented [MP36]: Libya dust?

Commented [MP37]: Libya dust? Please keep wording consistent

Commented [MP38]: I cannot see the double peak in the pre-edge region though I do not have a trained eye on this kind of graph. Maybe it isn't that distinct?



$$\sum_i RFe_i = k_i(pH, T) \times a(H^+)^{m_i} \times f_i \quad (1)$$

where RFe_i is the dissolution rate of individual mineral i , k_i is the rate constant (moles $Fe\ g^{-1}\ s^{-1}$), $a(H^+)$ is the H^+ activity in solution, m_i represents the empirical reaction order for protons. The function f_i ($0 \leq f_i \leq 1$) accounts for the suppression of mineral dissolution by competition for oxalate between surface Fe and dissolved Fe (Ito, 2015):

$$f_i = 0.17 \times \ln([lig] \times [Fe]^{-1})_i + 0.63 \quad (2)$$

in which, $[Fe]$ is the molar concentration ($mol\ L^{-1}$) of Fe^{3+} dissolved in solution, and $[lig]$ is the molar concentration of ligand (e.g., oxalate). f_i was set to 1 for the proton-promoted dissolution.

The scheme assumes 3 rate constants “fast”, “intermediate” and “slow” for the proton-promoted, and the proton + oxalate-promoted dissolution (Table 1). These were obtained by fitting the parameters to our measurements for Krakow ash in H_2SO_4 and $(NH_4)_2SO_4$ at pH 2-3, with and without oxalate (Experiments 2 and 3 in Table S1), which are shown in Fig. 6. The fast rate constant represents highly reactive Fe species such as amorphous Fe oxyhydroxides, Fe carbonates and Fe sulphates. The intermediate rate constant can be applied to nano-particulate Fe oxides, while more stable phases including for example Fealuminosilicate and crystalline Fe oxides have generally slower rate (Ito and Shi, 2016; Shi et al., 2011a; Shi et al., 2011b; Shi et al., 2015). Similarly, we predicted the dissolution kinetics of Aberthaw ash and Shandong ash (Figs. S3-S5). The dissolution kinetic of Krakow ash was calculated based also on the experimental results at pH 1.0, which

Commented [MP39]: In Fig 6a,c,d, the model seems to miss out on the rapid increase in Fe solubility (as if the solubility of Fe in the model had a threshold up to 24h-time, the latter which seem bias the model outcome). On the contrary the subsequent Fe dissolution (after 24h) seem exaggerated in the model compared to the slow increase in the experimental result.

A word on this?

Commented [MP40]: kinetics



is shown in Fig. S6 in comparison with kinetics predicted at pH 2.0 and pH 2.9 conditions.

The contribution of the oxalate-promoted dissolution to dissolved Fe was derived as the difference between the estimated dissolution rates for the proton + oxalate-promoted dissolution and the proton-promoted dissolution:

$$R_{Fe_i(oxalate)} = R_{Fe_i(proton + oxalate)} - R_{Fe_i(proton)} \quad (3)$$

The Fe dissolution rates were predicted at a wider range of pH using Eq. (1) and Eq. (3) and the parameters in Table 1:

$$R_{Fe_i} = R_{Fe_i(proton + oxalate)} \text{ when } R_{Fe_i(oxalate)} < 0 \quad (4)$$

Since $R_{Fe_i(oxalate)}$ is less than 0 at low pH (< 2), this equation applies to highly acidic conditions. As a result, the predicted amount of dissolved Fe was smaller when using the dissolution rate for the proton + oxalate-promoted dissolution, $R_{Fe_i(proton + oxalate)}$, rather than the rate for the proton-promoted dissolution, $R_{Fe_i(proton)}$, at pH < 2. Accordingly, the dissolution rate, R_{Fe_i} , was less dependent on the pH compared to $R_{Fe_i(proton)}$ at highly acidic conditions, possibly due to the competition for the formation of surface complexes.

At pH > 2 when oxalate does promote Fe dissolution, the following equation applies:

$$R_{Fe_i} = R_{Fe_i(proton)} + R_{Fe_i(oxalate)} \text{ when } R_{Fe_i(oxalate)} > 0 \quad (5)$$

4.2 Surface concentration of dissolved Fe over the Bay of Bengal

The new dissolution scheme was applied in the IMPACT atmospheric chemistry transport model to predict the surface concentration of dissolved Fe in atmospheric particles collected over the Bay of Bengal, which is an area for which there are



486 detailed field measurements available (Bikkina et al., 2020; Kumar et al., 2010;
487 Srinivas and Sarin, 2013; Srinivas et al., 2012) and multi-modelling analyses have
488 been done (Ito et al., 2019). It thus represents a test for our experimental results in
489 actual field conditions. Three sensitivity simulations were performed to explore the
490 ~~effects of the~~ uncertainties associated with the dissolution schemes and
491 mineralogical component of Fe. In addition, the former setting (Ito et al., 2021a)
492 was used in the IMPACT model for comparison.

493 In sensitivity Test 0, the total ~~anthropogenic~~ Fe emission ~~in aerosols~~ was estimated
494 using Fe emission factors by each sector such as energy, heavy industry, and iron
495 and steel industry for the simulation years (Ito et al., 2018), whereas in sensitivity
496 Test 1, Test 2, and Test 3, the mineral specific emission inventory for the year 2010
497 by Rathod et al. (2020) was used. In Test 0, we ran the model without the upgrades
498 of the dissolution scheme discussed in section 2.4, and apply in addition the
499 photoinduced dissolution scheme for both combustion and dust aerosols (Ito, 2015;
500 Ito and Shi, 2016), which was turned off in Test 1, Test 2, and Test 3 due to the lack
501 of laboratory measurements under high ionic strength. To estimate the aerosol pH,
502 we applied a H⁺ activity coefficient of 1 for Test 0, while the mean activity
503 coefficient from Pye et al. (2020) was used for the other tests. The dissolution rate
504 was assumed as pH-independent for highly acidic solutions (pH < 2) (Ito, 2015) in
505 Test 0, based on the laboratory measurements in Chen et al. (2012), while no pH
506 threshold was considered in Test 1, Test 2, and Test 3 as the total dissolution
507 (proton + oxalate) was suppressed at pH < 2 from the predicted dissolution rate.

508 In Test 1, we used the new dissolution scheme accounting for the proton- and
509 oxalate- promoted dissolution of Krakow ash for all combustion aerosols in the
510 model (Table 1). The dissolution kinetics was calculated using the mineral-specific

Formatted: Strikethrough

Formatted: Strikethrough

Deleted: anthropogenic

Commented [MP41]: Would a table help better understanding the different model test-runs?



inventory for anthropogenic Fe emissions (Rathod et al., 2020). The Fe composition of wood was used for open biomass burning (Matsuo et al., 1992). In this simulation, 3 Fe pools were considered. Sulphate Fe in Rathod et al. (2020) was assumed as fast pool, magnetite Fe as intermediate pool, hematite and Fe-aluminosilicate as slow pool. In Test 2, we calculated the dissolution kinetics only considering the proton-promoted dissolution. In Test 3, the Fe pools were as determined here for Krakow ash: ascorbate Fe (FeA) as fast pool, magnetite Fe (FeM) as intermediate pool, hematite plus goethite Fe (FeD) and other Fe as slow pool (Fig. 5). FeA contains highly reactive Fe species with fast dissolution rates (Raiswell et al., 2008; Shi et al., 2011b). FeM appeared to work well for the different fly ash samples in the dissolution scheme as intermediate Fe pool. FeD is associated with crystalline Fe oxides and a predominant proportion of this is highly insoluble (Raiswell et al., 2008; Shi et al., 2011b), thus it was considered as slow pool in the dissolution scheme. We assumed other Fe to be mostly as-Fe-bearing aluminosilicates and considered this as slow Fe pool.

The temporally and regionally averaged, model-calculated surface concentration of aerosol Fe (Fig. 7), dissolved Fe (Fig. 8) and Fe solubility (Figs. 9 and S7) for the fine mode (PM_{2.5}) along the cruise tracks were compared with the measurements over the Bay of Bengal for the period extending from 27 December 2008 to 26 January 2009 (Bikkina et al., 2020). The average aerosol Fe concentration observed over the Bay of Bengal varies from $145 \pm 144 \text{ ng m}^{-3}$ over the North Bay of Bengal (27 December 2008 - 10 January 2009) to $55 \pm 23 \text{ ng m}^{-3}$ over the South Bay of Bengal (11-26 January 2009) (Bikkina et al., 2020). In Fig. 7, the modelled aerosol Fe concentrations exhibit a similar variability to that of measurements with relatively higher values over the North Bay of Bengal ($101 \pm 57 \text{ ng m}^{-3}$ in Test 0, and $81 \pm 37 \text{ ng m}^{-3}$ in Test 1-3) compared to the South Bay of Bengal ($21 \pm 13 \text{ ng m}^{-3}$ in Test 0, and $34 \pm 25 \text{ ng m}^{-3}$ in Test 1-3). The model reproduced the source apportionment of Fe (Fig. 7) which is qualitatively derived from previous observational

Commented [MP42]: three

Commented [MP43]: which are mostly

Formatted: Strikethrough

Commented [MP44]: do you mean total surface aerosol Fe? Vs surface dissolved Fe? The term aerosol Fe is confusing as dissolved Fe also refers to Fe which is part of aerosol particles

Commented [MP45]: How did measurements differentiate surface aerosol Fe to total aerosol Fe and surface dissolved aerosol Fe to total dissolvable aerosol Fe? Are all the measurements really specific to the surface of aerosols or is dissolved Fe only assumed to originate from the surface of aerosol (what is the aerosol Fe component then?)?

Maybe better wording for each measurement is required for enhanced clarity.

Commented [MP46]: Total Fe in aerosols I assume?

Commented [MP47]: May I suggest that biomass burning is represented in orange or another colour as we cannot see it well as it currently is. Also, maybe instead of / in addition to plotting date as x axis, the location could be stated/ indicated (from the Northern Bay of Bengal to the South).



studies indicating that the aerosol Fe concentrations over the North Bay of Bengal are influenced by emissions of dust and combustion sources from the Indo-Gangetic Plain (Kumar et al., 2010), whereas combustion sources (e.g., biomass burning and fossil-fuel) from South-East Asia are dominant over the South Bay of Bengal (Kumar et al., 2010; Srinivas and Sarin, 2013). On the other hand, the model could not reproduce the peak in total Fe concentration (1.8% of Fe content in PM_{2.5} sample) reported around 29 December 2008. The total Fe observed in PM_{2.5} (613 ng m⁻³) is higher than that in PM₁₀ (430 ng m⁻³) (Srinivas et al., 2012). This may be due to the measurement uncertainty including sample collection with two different high-volume samplers (Kumar et al., 2010).

The average dissolved Fe concentration in aerosols measured over the North Bay of Bengal (16 ± 9 ng m⁻³) is slightly lower than that over the South Bay of Bengal (18 ± 10 ng m⁻³) (Bikkina et al., 2020). The model prediction of dissolved Fe over the North Bay of Bengal was 6 ± 2 ng m⁻³ Fe in Test 0, 21 ± 10 ng m⁻³ in Test 1, and 31 ± 28 ng m⁻³ in Test 2, and 13 ± 10 ng m⁻³ in Test 3. The aerosol dissolved Fe estimated over the South Bay of Bengal was 6 ± 1 ng m⁻³ in Test 0, 15 ± 10 ng m⁻³ in Test 1, 32 ± 22 ng m⁻³ in Test 2, and 12 ± 7 ng m⁻³ in Test 3. In Fig. 8, our model results show that the contribution of mineral dust to aerosol dissolved Fe was higher over the North Bay of Bengal ($14\% \pm 6\%$ in Test 1, $28\% \pm 34\%$ in Test 2, and $33\% \pm 26\%$ in Test 3) compared to the South Bay of Bengal ($3\% \pm 1\%$ in Test 1, $1\% \pm 1\%$ in Test 2, and $3\% \pm 1\%$ in Test 3). Overall, anthropogenic combustion sources were dominant over the Bay of Bengal accounting for $84\% \pm 12\%$ in Test 1, $72\% \pm 29\%$ in Test 2, and $69\% \pm 24\%$ in Test 3 of the aerosol dissolved Fe. Moreover, after 22 January 2009, the contribution of open biomass burning sources increased up to 47% in Test 1, 64% in Test 2, and 60% in Test 3 (Fig. 8).

Commented [MP48]: This peak is quite large for reflecting measurement uncertainty isn't it? Have you checked whether this point may be the result of a specific weather event (fire emission for example, such a peak may be visible from satellite observation) or may originate from a single sample contamination (in this case it should be discarded).

Commented [MP49]: dFe concentrations in aerosols seem to fluctuate a lot throughout the sampling transect. I would personally use median value rather than average for aerosols to avoid being biased by very low/high data points. The lowest dissolved Fe data are towards the right-hand side of the graph which I understood as "southern Bay of Bengal" but with no spatial indication on the graph I may have misinterpreted the data.

Deleted: aerosol



The aerosol Fe solubility measured over the South Bay of Bengal is higher than that over the North Bay of Bengal, respectively $32\% \pm 11\%$ and $15\% \pm 7\%$ (Bikkina et al., 2020), and model estimates showed a similar trend (Fig. S7). In Fig. S7, the calculated average Fe solubility over the North Bay of Bengal in Test 3 ($18\% \pm 10\%$) was in good agreement with observations, while lower Fe solubility was estimated in Test 0 ($8\% \pm 5\%$) and higher values were obtained for Test 1 ($28\% \pm 8\%$). The aerosol Fe solubility over the South Bay of Bengal was better captured in Test 1 ($43\% \pm 4\%$) and Test 3 ($39\% \pm 7\%$), whereas Test 0 showed higher variability ($38\% \pm 22\%$). The proton-promoted dissolution scheme in Test 2 significantly overestimated the Fe solubility over the Bay of Bengal (Figs. 9 and S7). The aerosol Fe solubility was largely overestimated in all scenarios after 22 January 2009, as open biomass burning sources become dominant (Fig. 8). The comparison between observations and model predictions of Fe solubility over the Bay of Bengal is shown in Fig. 9. The agreement between measurements and model predictions was the best in Test 1 and Test 3. These exhibited good correlation with observations ($R = 0.60$ in Test 1 and $R = 0.51$ in Test 3), and the lowest centred root-mean-square (RMS) difference between the simulated and observed aerosol Fe solubilities ($RMS = 16$ in Test 1 and $RMS = 14$ in Test 3). In Test 0, the model estimates showed higher difference from observations ($RMS = 22$) and poor correlation ($R = 0.30$).

5 Discussion

5.1 Dissolution behaviour of Fe in CFA

In this study, the Fe dissolution kinetics of CFA samples from UK, Poland and China was investigated under simulated atmospheric acidic conditions. A key parameter in both the atmosphere and the simulation experiments is the pH of the water interacting with the CFA particles. The lower the pH of the experimental solution the faster the dissolution and eventually the higher the amount of Fe

Commented [MP50]: I would personally have chosen Fig S7 to display on the ms instead of Fig 9. Indeed, Fig S7 as it shows the performance of each test-run to reproduce the observational data. Fig 9 is great but a little complex to interpret and to assess the model performance from.



dissolved. Our results showed a strong pH dependence in low ionic strength conditions, with higher dissolution rate at lower pH. For example, reducing the solution pH from 2.7 to 2.1, the Fe solubility of Krakow ash increased by a factor of 4 (Fig. 1a) over the duration of the experiments, while the Fe solubility of Aberthaw and Shandong ash increased by 9-10 times from pH 2.9 to pH 2.2 (Figs. 1b-c). This enhancement is higher than that observed in studies conducted on mineral dust samples, which showed that one pH unit can lead to 3-4 times difference in dissolution rates (Ito and Shi, 2016; Shi et al., 2011a). Furthermore, Chen et al. (2012) reported that the Fe solubility of the certified CFA 2689 only increased by 10% from pH 2 to pH 1, after 50 hours of dissolution in acidic media. The Fe solubility of CFA (PM₁₀ fractions) after 6 hours at pH 2 was 6%-10% for Aberthaw and Shandong ash respectively, and 28% for Krakow ash (Fig. 1). These values are higher than the Fe solubilities measured by Fu et al. (2012), who reported 2.9%-4.2% Fe solubility in bulk CFA from three coal-fired power plants in China after 12-hour leaching at pH 2. This suggest that Fe in our CFA samples initially dissolved faster than those used in Fu et al. (2012). The Fe solubility after 72-hour leaching in H₂SO₄ at around pH 2 varied from around 12% and 17% (Aberthaw and Shandong ash) to 34% (Krakow ash). These values are at the lower end of the range or below those reported in Chen et al. (2012), who measured a Fe solubility of ~20%-70% in certified CFA samples after accumulated acid dissolution of 72 hours at pH 2. These results suggest that there are considerable variabilities in the pH dependent dissolution of Fe in CFA. Our results showed that high ionic strength has a major impact on dissolution rates of CFA at low pH (i.e., pH 2-3). The Fe solubility of CFA increased by approximately 20%-40% in the presence of 1 M (NH₄)₂SO₄ at around pH 2 over

Commented [MP51]: Different samples and leaching protocols and leaching solutions will also play a role in the differences highlighted here and above. 3 CFAs in this study already have different reactions to the same protocol, likely due to different mineralogy and different degree of combustion (this study has not addressed possible incomplete combustion from the sampled power plants)

Commented [MP52]: Please see comment above, I believe many factors come into play and this conclusion cannot be drawn without acknowledging these parameters.

Commented [MP53]: Here may also be a good time to mention other parameters that come into play apart from pH. Reminding the readers the all these studies are not strictly comparable to one another.

Commented [MP54]: Is that the percentage increase or the final Fe solubility. Maybe the "from x%...to x%" is less prone to misunderstanding.



the duration of the experiments, and by a factor ~~from 3~~ to 7 at around pH 3 conditions (Fig. 1). At high ionic strength, the activity of ions in solution is reduced, thus, in order to maintain similar pH conditions, the H^+ concentration has to be increased (Table S1). Although Fe dissolution was primarily controlled by the concentration of H^+ , the high concentration of sulphate ions could be also an important factor contributing to Fe dissolution, in particular when the concentration of H^+ in the system was low (e.g., pH 3). Previous research found that the high ability of anions to form soluble complexes with metals can enhance Fe dissolution (Cornell et al., 1976; Cornell and Schwertmann, 2003; Furrer and Stumm, 1986; Hamer et al., 2003; Rubasinghege et al., 2010; Sidhu et al., 1981; Surana and Warren, 1969). Sulphate ions adsorbed on the particles surface form complexes with Fe (e.g., Rubasinghege et al., 2010). This may increase the surface negative charge favouring the absorption of H^+ and thereby increase the dissolution rate. In addition, the formation of surface complexes may weaken the bonds between Fe and the neighbouring ions (Cornell et al., 1976; Furrer and Stumm, 1986; Sidhu et al., 1981). Cwiertny et al. (2008) reported that at pH 1-2 the high ionic strength generated by NaCl up to 1 M did not influence Fe dissolution of mineral dust particles. However, Ito and Shi (2016) showed that the high ionic strength resulting from the addition of 1 M $(NH_4)_2SO_4$ in leaching solutions at pH 2-3 enhanced the Fe dissolution of dust particles, which was also observed here for the CFA samples. Borgatta et al. (2016) compared the Fe solubility of CFA from USA Midwest, North-East India, and Europe in acidic solution (pH 1-2) containing 1 M NaCl. The Fe solubility measured after 24 hours varied from 15% to 70% in different CFA (bulk samples) at pH 2 with 1 M NaCl, which was considerably higher than that observed at pH 2 with 1 M $NaNO_3$ (<20%) (Kim et al., 2020). Both studies did not investigate the impact of ionic strength on the dissolution behaviour, i.e., by comparing the dissolution at low and high ionic strength. Note that both studies did not specify how the pH conditions were

Formatted: Strikethrough

Commented [MP55]: Thereby Fe dissolution at the surface of particles



maintained at pH 2. Here, we considered the most important sources of high ionic strength in aerosol water and simulated Fe dissolution in the presence of $(\text{NH}_4)_2\text{SO}_4$ and $\text{H}_2\text{C}_2\text{O}_4$ under acidic conditions. We emphasize that the pH under high ionic strength here is estimated from a thermodynamic model, similar to those implemented in the IMPACT model.

The presence of oxalate enhanced Fe dissolution in Krakow and Aberthaw ash but not in Shandong ash at around pH 2 (Fig. 2). The effect of oxalate on the Fe dissolution kinetics has also been studied by Chen and Grassian (2013) at pH 2 (11.6 mM $\text{H}_2\text{C}_2\text{O}_4$). After 45-hour leaching, the Fe solubility of the certified CFA 2689 increased from 16% in H_2SO_4 at pH 2 to 44% in $\text{H}_2\text{C}_2\text{O}_4$ at the same pH (Chen and Grassian, 2013). Therefore, the enhancement in Fe solubility of CFA in the presence of oxalate observed in this study (from no impact in Shandong ash to doubled dissolution in Krakow ash) is lower than that reported for the certified CFA 2689, which was around by 2.8 times (Chen and Grassian, 2013). Since no data are available in Chen and Grassian (2013), we are unable to make a comparison with the other two certified CFA samples. The Fe solubility of Krakow ash after 48-hour leaching at pH 1.9 with 0.01 M $\text{H}_2\text{C}_2\text{O}_4$ (Fig. 2a) was 53%, which is within the range of Fe solubilities observed in Chen and Grassian (2013) for the certified CFA samples at similar pH and $\text{H}_2\text{C}_2\text{O}_4$ concentrations (from 44% to 78%), whereas the Fe solubility of Aberthaw and Shandong ash (Figs. 2b-c, 18%-17% after 48-hour leaching at pH 2.0 with 0.01 M $\text{H}_2\text{C}_2\text{O}_4$) was considerably lower than that of certified CFA (Chen and Grassian, 2013). These results suggest a large variability in the effects of oxalate on the Fe dissolution rates in different types of CFA.

Our results also indicated that high $(\text{NH}_4)_2\text{SO}_4$ concentrations suppress oxalate-promoted Fe dissolution of CFA (Fig. 2), which was not considered in previous

Commented [MP56]: 'is lower than the 2.8 time increase in Fe solubility reported for the certified ...'

Formatted: Strikethrough

Formatted: Space After: 0,55 pt, Line spacing: Multiple 1,5 li



research. At pH 1.9 in the presence of oxalate, the Fe solubility of Krakow ash decreased by around 10% after the addition of $(\text{NH}_4)_2\text{SO}_4$, while the Fe solubility of Aberthaw ash decreased by 35% (Fig. 2). We used the E-AIM model to estimate the concentration of oxalate ions and their activity (Table S2). The pH influences the speciation of $\text{H}_2\text{C}_2\text{O}_4$ in solution (e.g., Lee et al., 2007). $\text{H}_2\text{C}_2\text{O}_4$ is the main species below pH 2, whereas HC_2O_4^- is dominant between pH 1–4. Above pH 4, $\text{C}_2\text{O}_4^{2-}$ is the principal species. In our experiments, $\text{H}_2\text{C}_2\text{O}_4$ is mainly as HC_2O_4^- at around pH 2 (Experiments 3–4 in Table S2). In the presence of $(\text{NH}_4)_2\text{SO}_4$, the activity coefficient of HC_2O_4^- was reduced by approximately 35–38% (Experiments 3 in Table S2). Increasing the ionic strength lowers the activity of the oxalate ions, but at the same time favours the dissociation of the acid. At around pH 2 conditions, the E-AIM model estimated that the activity of $\text{C}_2\text{O}_4^{2-}$ was reduced by around one order of magnitude in the presence of $(\text{NH}_4)_2\text{SO}_4$, while its concentration increased 12–15 times (Experiments 3 in Table S2). The adsorption of anions can reduce oxalate adsorption on the particle surface due to electrostatic repulsion which results in slower dissolution rates (Eick et al., 1999). Precipitation of ammonium hydrogen oxalate ($\text{NH}_4\text{HC}_2\text{O}_4$) can also occur in the system, but this is very soluble and easily re-dissolves forming soluble oxalate species (Lee et al., 2007). We speculate that the high concentration of sulphate ions is likely to be responsible for inhibiting the oxalate-promoted dissolution by reducing oxalate adsorption on the particle surface. At pH 1 in the presence of oxalate, increasing the concentration of $(\text{NH}_4)_2\text{SO}_4$ from 0.5 M to 1.5 M did not affect the Fe dissolution behaviour of the CFA samples (Fig. 4). As previously discussed, the adsorption of sulphate ions on the particle surface may inhibit oxalate-promoted dissolution. However, once the saturation coverage is reached, increasing the concentration of anions has no further effect on the dissolution rate (Cornell et al., 1976). Fe speciation is an important factor affecting the Fe dissolution behaviour. CFA particles have very different chemical and physical properties depending on

Deleted: ¶

Commented [MP57]: pH 2–4?

Commented [MP58]: For Fe at the surface of aerosols



example₂ on the nature of coal burned, combustion conditions, cooling process and particle control devices implemented at the power stations (e.g., Blissett and Rowson, 2012; Yao et al., 2015). This is likely the reason why the Fe speciation observed in the CFA samples analysed in this study from different location varied considerably (Fig. 5). In the CFA samples, the Fe dissolution curves for different pH and ionic strengths generally showed the greatest rate of Fe release within the first 2 hours, followed by a slower dissolution, reaching almost a plateau at the end of the experimental run. This indicates the presence of multiple Fe phases in CFA particles with a wide range of reactivity. Initially, highly reactive phases were the main contribution to dissolved Fe. As the dissolution continued, more stable phases became the dominant source of dissolved Fe (Shi et al., 2011a). SEM analysis conducted on CFA samples showed that CFA particles are mostly spherical (e.g., Chen et al., 2012; Dudas and Warren, 1987; Valeev et al., 2018; Warren and Dudas, 1989) with Fe oxide aggregates on the surface (Chen et al., 2012; Valeev et al., 2018). The analysis of the CFA samples processed in aqueous solution at low pH suggests that initially Fe dissolved from the reactive external glass coating (Dudas and Warren, 1987; Warren and Dudas, 1989) and from the Fe oxide aggregates on the particle surface (Chen et al., 2012; Valeev et al., 2018). Subsequently, Fe is likely realised from the structure of the aluminium silicate glass (Chen et al., 2012; Dudas and Warren, 1987; Valeev et al., 2018; Warren and Dudas, 1989), and crystalline Fe oxide phases (Warren and Dudas, 1989). Overall, Krakow ash showed the fastest dissolution rates, but the dissolution of highly reactive Fe species as FeA is insufficient to account for the high Fe solubility observed at low pH. Our results showed that once the FeA dissolved, additional Fe was dissolved from more refractory Fe phases. The modelled dissolution kinetics obtained using FeM as

Commented [MP59]: Less soluble phases? I believe they are all chemically stable but show different reactivity toward the leaching media



intermediate pool were in good agreements with measurements (Figs. S3-S6). FeM is likely to be primary magnetite but may contain a fraction of the more reactive aluminosilicate glass. Our model results suggest that magnetite in CFA particles may be more soluble than has been shown in Marcotte et al. (2020). It is possible that in real CFA samples the physicochemical properties of minerals, including for example crystal size, degree of crystallinity, cationic and anionic substitution in the lattice which influence the Fe dissolution behaviour (e.g., Schwertmann, 1991), are likely to be different from those of the reference minerals analysed in Marcotte et al. (2020). In order to estimate in detail the relative contribution of different mineral phases present in CFAs to dissolved Fe, most detailed work would be needed to determine Fe mineral phases in pristine and processed CFA particles.

Finally, the modelled dissolution kinetics obtained using the new dissolution scheme for CFA (Table 1) showed better agreement with laboratory measurements than when using the original scheme (Ito, 2015) (Figs. S8 and S9). In Fig. S8, we compared the Fe dissolution kinetics of Krakow ash at around pH 2 and 3 with 1 M (NH₄)₂SO₄ calculated using the proton-promoted dissolution scheme in Table 1 with the dissolution kinetics calculated at similar pH but using the proton-promoted dissolution scheme for combustion aerosols in Ito (2015) (Table S3). The dissolution scheme in Ito (2015) was based on laboratory measurements conducted at low ionic strength (Chen et al., 2012) and assumed a single Fe phase in combustion aerosol particles, while the new dissolution scheme considered the high ionic strength of aerosol water and assumed three rate constants, for fast, intermediate and slow kinetics of the different Fe phases present in CFA particles. The Fe dissolution kinetics obtained using the new dissolution scheme showed a better agreement with measurements and was enhanced compared to the model estimates obtained using the original dissolution scheme (Ito, 2015) for low ionic strength conditions (Fig. S8). Figure S9 shows the Fe dissolution kinetics of

Deleted: mineral

Commented [MP60]: What is a pristine CFA? Aren't CFAs always the result of a combustion process (therefore, 'processed' particles)? Not sure about the wording used.

Commented [MP61]: May be worth displaying in the manuscript



753 Krakow ash at pH 2.0 and 2.9 with 0.01 M $\text{H}_2\text{C}_2\text{O}_4$ and 1 M $(\text{NH}_4)_2\text{SO}_4$ calculated
754 using the proton- and oxalate-promoted dissolution scheme in Table 1 and the
755 dissolution kinetics calculated at similar pH and $\text{H}_2\text{C}_2\text{O}_4$ concentration but using the
756 scheme in Ito (2015) (i.e., single phase dissolution, see Table S3). The Fe
757 dissolution kinetics predicted using the new dissolution scheme had a much better
758 agreement with measurements. Figure S9c shows the suppression of the oxalate-
759 promoted dissolution at pH 2.0 and high $(\text{NH}_4)_2\text{SO}_4$ concentrations. At pH 2, the
760 protonpromoted dissolution was comparable to the proton + oxalate-promoted
761 dissolution (Fig. S9c), with $R_{\text{Fe}(\text{oxalate})}$ close to zero (see Eq. 3). At pH 2.9, the
762 proton + oxalate-promoted dissolution was higher than the proton + oxalate-
763 promoted dissolution (Fig. S9d), with $R_{\text{Fe}(\text{oxalate})} > 0$ (Eq. 5).
764 Moreover, the new 3-step dissolution scheme better captured the initial fast
765 dissolution of CFA (Figs. 2-3) which was also observed in previous research
766 (Borgatta et al., 2016; Chen et al., 2012; Chen and Grassian, 2013; Fu et al., 2012;
767 Kim et al., 2020) (except for the certified CFA 2689 in Chen et al. (2012) which
768 showed increasing dissolution rates over the duration of the experiment).
769 Furthermore, the new scheme enabled us to account for the different Fe speciation
770 determined in the CFA samples, which could be a key factor contributing to the
771 different Fe dissolution behaviour observed in the present study and in literature
772 (Borgatta et al., 2016; Chen et al., 2012; Chen and Grassian, 2013; Fu et al., 2012;
773 Kim et al., 2020). In Figs. S3S5, the dissolution kinetics of Aberthaw and Shandong
774 ash calculated using the dissolution rates in Table 1 and the Fe phases determined in
775 the samples showed a good agreement with measurements.



5.2 Comparison with mineral dust

High ionic strength also impacted the dissolution rates of the Saharan dust sample at low pH (Fig. S10). At around pH 2 conditions, the proton-promoted Fe dissolution of Libya dust was enhanced by ~40% after the addition of $(\text{NH}_4)_2\text{SO}_4$. At around pH 2 and with 0.01 M $\text{H}_2\text{C}_2\text{O}_4$, the Fe solubility of Libya dust decreased by ~30% in the presence of $(\text{NH}_4)_2\text{SO}_4$. Overall, the Fe solubility of Libya dust was lower compared to that observed in the CFA samples. After 168 hour-leaching at pH 2.1 with 1 M $(\text{NH}_4)_2\text{SO}_4$, the Fe solubility of Libya dust was 7.2% (Fig. S10), which was from around 3 to 7 times lower compared to that of the CFA samples (Fig. 1). At around pH 2 conditions in the presence of oxalate and high $(\text{NH}_4)_2\text{SO}_4$ concentration, the Fe solubility of Libya dust rose to ~13.6% (Fig. S10), which is still 4 times lower than that of Krakow ash and around 1.5 lower than Aberthaw and Shandong ash (Fig. 2). The Fe solubilities of Libya dust observed in this study are comparable with those of the Tibesti dust in Ito and Shi (2016) at similar experimental conditions.

The enhanced Fe solubility in CFA compared to mineral dust could be primarily related to the different Fe speciation (Figs. 5 and S2). CFA contained more highly reactive Fe and magnetite but less hematite and goethite than mineral dust.

Although mineral dust is the largest contribution to total aerosol Fe while CFA accounts for only a few percent, atmospheric processing of CFA may result in a larger than expected contribution of bioavailable Fe deposited to the surface ocean. It is thus important to quantify the amount and nature of CFA in atmospheric particles.

5.3 Comparison of modelled Fe solubility with field measurements

The model results obtained using the emission inventory from Rathod et al. (2020) and the new dissolution scheme for the proton + oxalate-promoted dissolution (Table 1) in Test 1 and Test 3 provided a better estimate of dissolved Fe over the Bay of Bengal than the other tests (Figs. 8, 9, and S7). At the same time, the new

Commented [MP62]: Libya dust?

Commented [MP63]: Could you provide the solubility in “” please so the reader have an idea of the impact of each treatment ?

Deleted: ¶



805 model improved the agreement of aerosol Fe solubility from Test 0 ($70\% \pm 4\%$) to
806 Test 1 ($44\% \pm 3\%$) and Test 3 ($48\% \pm 1\%$) with the field data ($25\% \pm 3\%$) but still
807 overestimated it after 22 January 2009, when open biomass burning sources become
808 dominant (Fig. 8). This could be due to the unrepresentative Fe speciation used in
809 Test 1 and Test 3 for biomass burning over the Bay of Bengal. To reduce the
810 uncertainty in model predictions, emission inventories could be improved through a
811 comprehensive characterization of Fe species in combustion aerosol particles.
812 The revised model also enabled us to predict sensitivity to a more dynamic range of
813 pH changes, particularly between anthropogenic combustion and biomass burning.
814 The results show that the proton-promoted dissolution scheme in Test 2
815 significantly overestimated aerosol dissolved Fe (Figs. 8, 9 and S7), which indicates
816 the suppression of the proton + oxalate-promoted dissolution at $\text{pH} < 2$. In Fig. 10,
817 the model estimates of surface concentration of dissolved Fe over the Bay of Bengal
818 considerably improved in Test 1 compared to Test 0. The model results in Test 1
819 also indicate a larger contribution of pyrogenic dissolved Fe over regions with
820 strong anthropogenic source such as East Asia, but a smaller contribution
821 downwind from tropical biomass burning regions (Fig. 11). We demonstrated that
822 the implementation of the new Fe dissolution scheme, including a rapid Fe release
823 at the initial stage and highly acidic conditions, enhanced the model estimates.
824 However, in Test 1, we turned off the photo-reductive dissolution scheme (Ito,
825 2015), which was based on the laboratory measurements in Chen and Grassian
826 (2013). To determine the photoinduced dissolution kinetic of CFA particles it is
827 necessary to account for the effect of high concentration of $(\text{NH}_4)_2\text{SO}_4$ on photo-
828 reductive dissolution rate which should be considered in future research.

Commented [MP64]: Is that a certainty related in the study?

Commented [MP65]: This source wasn't assed in this study. Moreover, the sentence just above raise awareness on the need for more investigation on BB. The revised model has improved modelling of anthropogenic aeolian Fe dissolution.

Commented [MP66]: Did improve yes but the Test 1 model run is still quite off for a range of datapoints

Commented [MP67]: Anthropogenic?

Commented [MP68]: No short conclusion?



Data availability statement

The new dissolution schemes for the proton-promoted and oxalate-promoted dissolution are reported in Table 1. Table S1 reports the concentrations of H_2SO_4 , $\text{H}_2\text{C}_2\text{O}_4$ and $(\text{NH}_4)_2\text{SO}_4$ in the experiment solutions, the original and final pH from model estimates (including H^+ concentrations and activities), and the pH measurements for the solution with low ionic strength. Table S2 contains the summary of the concentration and activity of total oxalate ions, $\text{C}_2\text{O}_4^{2-}$, and HC_2O_4^- in the experiment solutions calculated using the E-AIM model III. The observations of the surface concentration of aerosol Fe, dissolved Fe and Fe solubility for the fine mode ($\text{PM}_{2.5}$) over the Bay of Bengal are from Bikkina et al. (2020) and are available at <https://pubs.acs.org/doi/10.1021/acsearthspacechem.0c00063>. The Fe speciation, the measurements of the Fe dissolution kinetic, and the results of the IMPACT model for each sensitivity simulation (Test 0-3) can be downloaded at: <https://doi.org/10.25500/edata.bham.00000702>.

Author contributions

CB, ZS, and AI designed the experiments and discussed the results. ZS supervised the experimental and data analyses. CB conducted the experiments and the data analysis with contributions from ZS, AI, MDK and ND. ND, ZS and KI performed the XANES measurements. AI developed the model of the dissolution kinetics and performed the model simulations. Krakow and Aberthaw ash were provided by TJ, while Shandong ash was provided by WL. Soil 5 from Libya was collected by ND. CB prepared the article with contributions from MDK and all the other co-authors.

Competing interests

The authors declare that they have no conflict of interest.



Acknowledgments

CB is funded by the Natural Environment Research Council (NERC) CENTA studentship (grant no. NE/L002493/1). Support for this research was provided to AI by JSPS KAKENHI (grant no. 20H04329), Integrated Research Program for Advancing Climate Models (TOUGOU) (grant no. JPMXD0717935715) from the Ministry of Education, Culture, Sports, Science and Technology (MEXT), Japan. We acknowledge Diamond Light Source for time on Beamline/Lab I18 under the Proposals: SP22244-1; SP12760-1; SP10327-1.

Financial support

This research has been supported by the Natural Environment Research Council (grant no. NE/L002493/1), JSPS KAKENHI (grant no. 20H04329), the Integrated Research Program for Advancing Climate Models (TOUGOU) (grant no. JPMXD0717935715).

Table 1. Constants used to calculate Fe dissolution rates for fossil fuel combustion aerosols, based on laboratory experiments conducted at high ionic strength.

Stage	Kinetic	Scheme	Rate constant - $k(\text{pH}, T)^a$	m^c
I	Fast	Proton	$7.61 \times 10^{-6} \exp[E(\text{pH})^b \times (1/298 - 1/T)]$	0.241
II	Intermediate	Proton	$1.91 \times 10^{-7} \exp[E(\text{pH})^b \times (1/298 - 1/T)]$	0.195
III	Slow	Proton	$2.48 \times 10^{-7} \exp[E(\text{pH})^b \times (1/298 - 1/T)]$	0.843
I	Fast	Proton + Oxalate	$5.54 \times 10^{-6} \exp[E(\text{pH})^b \times (1/298 - 1/T)]$	0.209
II	Intermediate	Proton + Oxalate	$1.50 \times 10^{-7} \exp[E(\text{pH})^b \times (1/298 - 1/T)]$	0.091

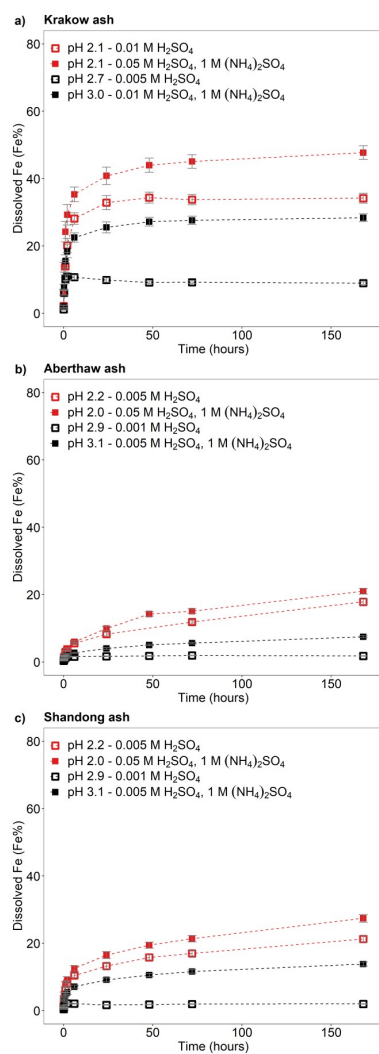


III	Slow	Proton + Oxalate	$1.77 \times 10^{-8} \exp[E(\text{pH})^b \times (1/298 - 1/T)]$	0.204
-----	------	------------------	---	-------

^a $k(\text{pH}, T)$ is the pH and temperature dependent ‘far-from-equilibrium’ rate constant (moles Fe g⁻¹ s⁻¹). The Fe dissolution scheme assumes 3 rate constants “fast”, “intermediate” and “slow” for the proton- and oxalate-promoted dissolution. The parameters were fit to our measurements for Krakow ash.

^b $E(\text{pH}) = -1.56 \times 10^3 \times \text{pH} + 1.08 \times 10^4$. The parameters were fit to the measurements for soils (Bibi et al., 2014).

^c m is the reaction order with respect to aqueous phase protons, which was determined by linear regression from our experimental data in the pH range between 2 and 3 for proton- and oxalate-promoted dissolution schemes.



<https://doi.org/10.5194/acp-2021-748>

Preprint. Discussion started: 30 September 2021

© Author(s) 2021. CC BY 4.0 License.



880 Figure 1: Fe dissolution kinetics of a) Krakow ash, b) Aberthaw ash and c) Shandong ash in H₂SO₄ solutions (open rectangles)
881 and with 1 M (NH₄)₂SO₄ (filled rectangles). The molar concentrations of H₂SO₄ and (NH₄)₂SO₄ in the experiment solutions are
882 shown. The final pH of the experiment solutions is also reported, which was calculated using the E-AIM model III for aqueous
883 solution (Wexler and Clegg, 2002) accounting for the buffer capacity of the CFA samples (Experiments 1-2 in Table S1). The
884 experiments conducted at around pH 2 are in red, while the experiments at around pH 3 are in black. The data uncertainty
885 was estimated using the error propagation formula.

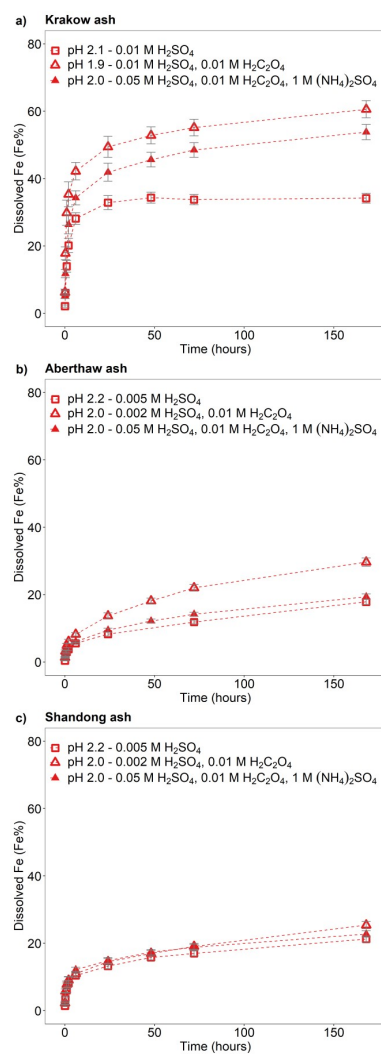




Figure 2: Fe dissolution kinetics of a) Krakow ash, b) Aberthaw ash, and c) Shandong ash in H_2SO_4 solutions at around pH 2 (red open rectangles), with 0.01 M $\text{H}_2\text{C}_2\text{O}_4$ (red open triangles), and 1 M $(\text{NH}_4)_2\text{SO}_4$ (red filled triangles). The molar concentrations of H_2SO_4 , $\text{H}_2\text{C}_2\text{O}_4$ and $(\text{NH}_4)_2\text{SO}_4$ in the experiment solutions are shown. The final pH of the experiment solutions is also reported, which was calculated using the E-AIM model III for aqueous solution (Wexler and Clegg, 2002) accounting for the buffer capacity of the CFA samples (Experiments 1, 3-4 at around pH 2). The data uncertainty was estimated using the error propagation formula.

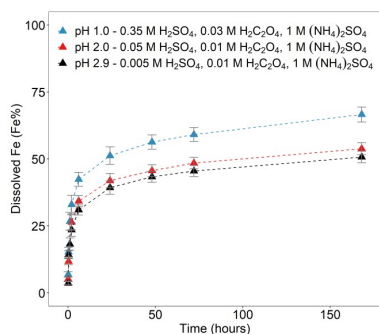


Figure 3: Fe dissolution kinetics of Krakow ash in H_2SO_4 solutions at pH 1.0 with 0.03 M $\text{H}_2\text{C}_2\text{O}_4$ and 1 M $(\text{NH}_4)_2\text{SO}_4$ (blue filled triangles), at pH 2.0 with 0.01 M $\text{H}_2\text{C}_2\text{O}_4$ and 1 M $(\text{NH}_4)_2\text{SO}_4$ (red filled triangles), and at pH 2.9 with 0.01 M $\text{H}_2\text{C}_2\text{O}_4$ and 1 M $(\text{NH}_4)_2\text{SO}_4$ (black filled triangles). The molar concentrations of H_2SO_4 , $\text{H}_2\text{C}_2\text{O}_4$ and $(\text{NH}_4)_2\text{SO}_4$ in the experiment solutions are shown. The final pH of the experiment solutions is also reported, which was calculated using the E-AIM model III for aqueous solution (Wexler and Clegg, 2002) accounting for the buffer capacity of the CFA samples (Experiment 7 at pH 1.0, Experiment 3 at pH 2.0, and Experiment 3 at pH 2.9 in Table S1). The data uncertainty was estimated using the error propagation formula.

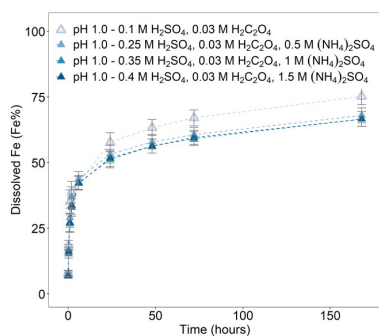


Figure 4: Fe dissolution kinetics of Krakow ash in H_2SO_4 solutions at pH 1.0 with 0.03 M $\text{H}_2\text{C}_2\text{O}_4$ and concentration of $(\text{NH}_4)_2\text{SO}_4$ from 0 to 1.5 M. The molar concentrations of H_2SO_4 , $\text{H}_2\text{C}_2\text{O}_4$ and $(\text{NH}_4)_2\text{SO}_4$ in the experiment solutions are shown. The final pH of the experiment solutions is also reported, which was calculated using the E-AIM model III for aqueous solution (Wexler and Clegg, 2002) accounting for the buffer capacity of the CFA samples (Experiments 5-8 in Table S1). The data uncertainty was estimated using the error propagation formula.

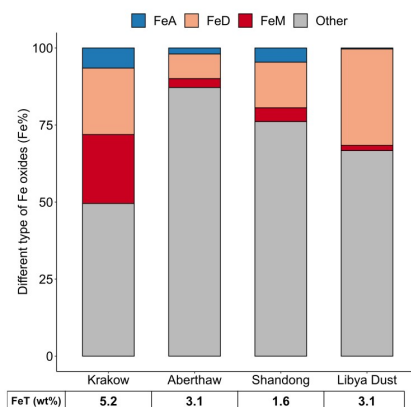


Figure 5: Percentages of ascorbate Fe (FeA), dithionite Fe (FeD), magnetite Fe (FeM) and other Fe to the total Fe (FeT) in the coal fly ash samples and mineral dust from Africa (Libya dust). The FeT (as %wt.) was given below each sample column. The data uncertainty was estimated using the error propagation formula: 4% for FeA/FeT, 11% for FeD/FeT, 12% for FeM/FeT, and 2 % for FeT.

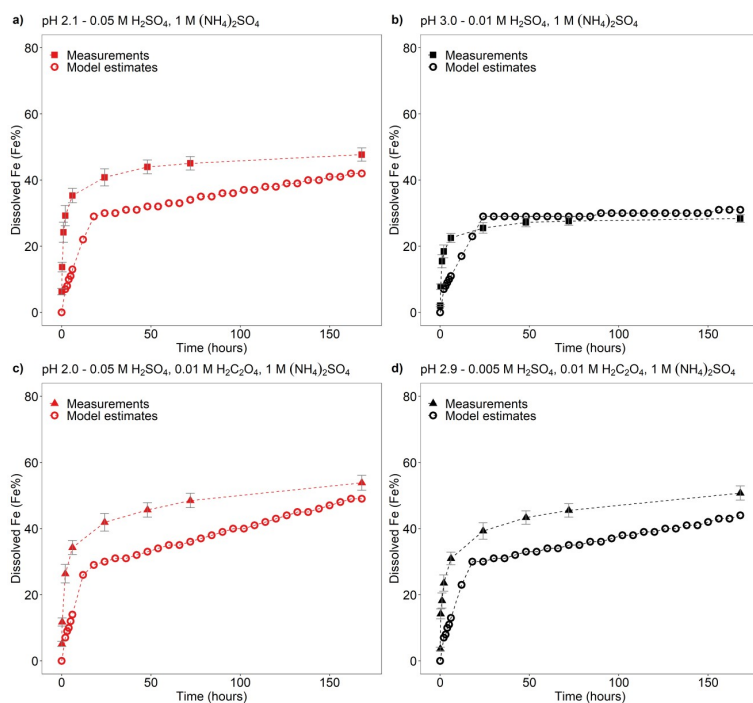
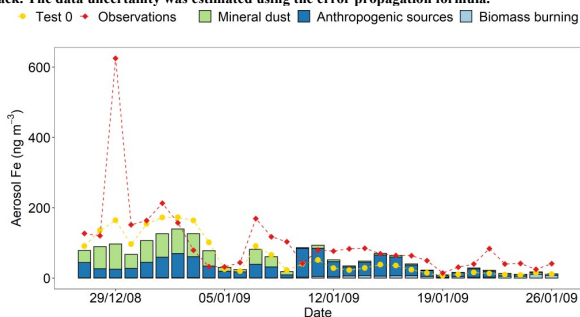


Figure 6: Comparison between the Fe dissolution kinetics of Krakow ash predicted using Eq. (1) and measured in H_2SO_4 solutions a-b) with 1 M $(\text{NH}_4)_2\text{SO}_4$, c-d) with 0.01 M $\text{H}_2\text{C}_2\text{O}_4$ and 1 M $(\text{NH}_4)_2\text{SO}_4$. The molar concentrations of H_2SO_4 , $\text{H}_2\text{C}_2\text{O}_4$ and $(\text{NH}_4)_2\text{SO}_4$ in the experiment solutions are shown. The final pH of the experiment solutions is also reported, which was calculated using the EAIM model III for aqueous solution (Wexler and Clegg, 2002) accounting for the buffer capacity of the CFA samples (Experiments 2-3 in Table S1). The experiments conducted at around pH 2 are in red, while the experiments at around pH 3 are in black. The data uncertainty was estimated using the error propagation formula.



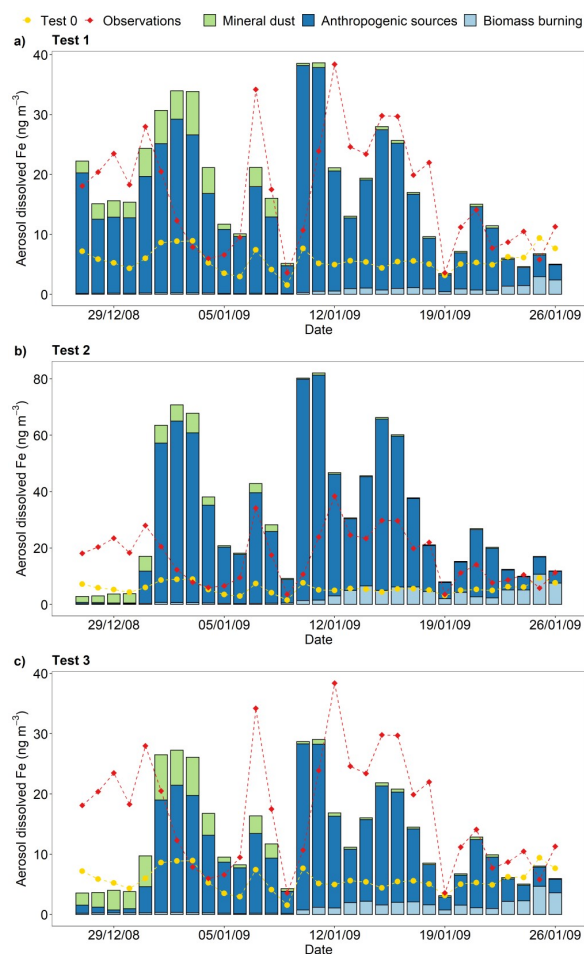
<https://doi.org/10.5194/acp-2021-748>

Preprint. Discussion started: 30 September 2021

© Author(s) 2021. CC BY 4.0 License.



619 **Figure 7: Surface concentration of Fe in $PM_{2.5}$ aerosol particles over the Bay of Bengal from 27 December 2008 to 26 January**
620 **2009. Observations are from Bikkina et al. (2020) (red filled diamonds). Aerosol Fe was calculated along the cruise tracks using**
621 **the IMPACT model. The total Fe emission in anthropogenic aerosols was estimated using Fe emission factors by each sector**
622 **such as energy, industry, and iron and steel industry for the simulation years (Ito et al., 2018) in sensitivity Test 0 (yellow filled**
623 **circles), while the mineral specific emission inventory for the year 2010 by Rathod et al. (2020) was used in the other tests. The**
624 **contribution of mineral dust sources, anthropogenic sources and biomass burning to total Fe is shown for Test 1-3.**



Commented [MP69]: BB could have been another colour (orange for example) for a better visual.

Figure 8: Surface concentration of dissolved Fe in $PM_{2.5}$ aerosol particles over the Bay of Bengal from 27 December 2008 to 26 January 2009. Observations are from Bikkina et al. (2020) (red filled diamonds). Aerosol dissolved Fe was calculated along the cruise tracks using the IMPACT model. In Test 0 (yellow filled circles), we ran the model without upgrades in the Fe dissolution scheme (Ito et al., 2021a), and applying the proton-promoted, oxalate-promoted and photoinduced dissolution schemes for combustion aerosols. The contribution of mineral dust sources, anthropogenic sources and biomass burning is shown for Test 1-3. The proton + oxalate dissolution scheme (Table 1) was applied in Test 1 and 3, while proton-promoted dissolution is used for Test 2. We adopted the mineral-specific inventory for anthropogenic Fe emissions (Rathod et al., 2020) in Test 1 and 2. In Test 3, the Fe speciation of Krakow ash was used for all combustion sources.

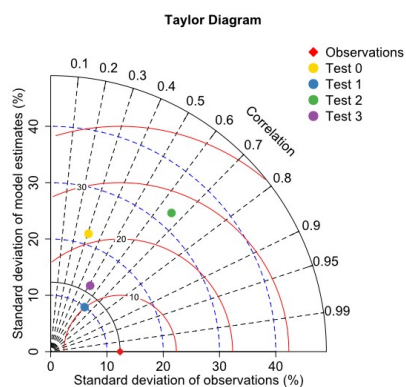
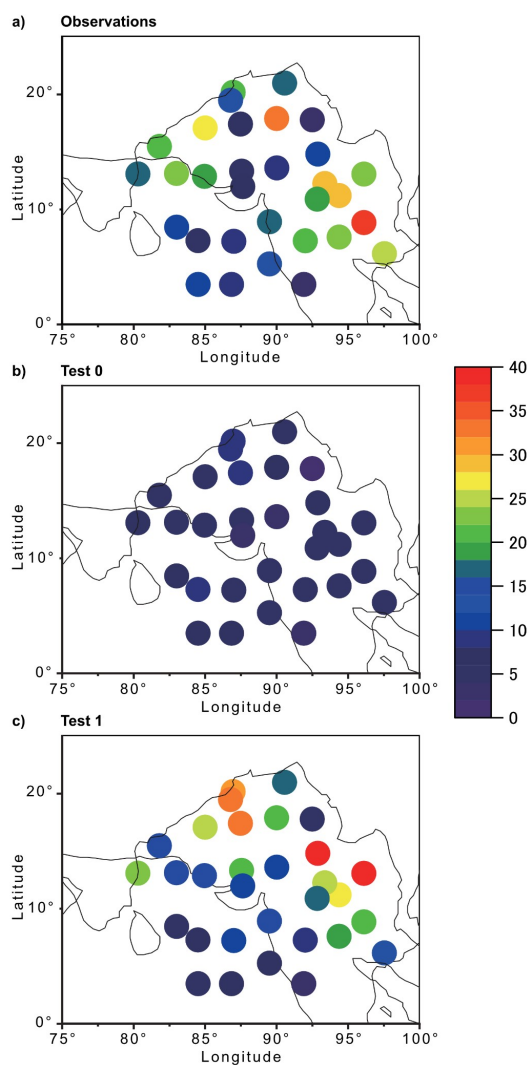


Figure 9: Comparison between observations and model estimates of Fe solubility in $\text{PM}_{2.5}$ aerosol particles over the Bay of Bengal from 27 December 2008 to 26 January 2009. Observations are from Bikkina et al. (2020). Aerosol Fe solubility was calculated along the cruise tracks using the IMPACT model. The Taylor diagram summarizes the statistics for the comparison between observations of aerosol Fe solubility and the different simulations (Test 0-3). The dashed curves in blue indicate the standard deviation values. The curves in red denote the root-mean-squared difference between the observational data and the model predictions. The dashed lines in black represent the correlation coefficients.



Commented [MP70]: Can the color scale be improved in the dark blue and purple shades?

641

642 **Figure 10:** Surface concentration of dissolved Fe in $PM_{2.5}$ aerosol particles over the Bay of Bengal from 27 December 2008 to 26
643 January 2009. a) Observations from Bikina et al. (2020). b-c) Aerosol dissolved Fe calculated along the cruise tracks using the
644 IMPACT model. In Test 0, we ran the model without upgrades in the Fe dissolution scheme (Ito et al., 2021a) and applying the



proton-promoted, oxalate-promoted and photoinduced dissolution schemes for combustion aerosols Table S3 (Ito, 2015). The proton + oxalate dissolution scheme (Table 1) was applied in Test 1 and we adopted the mineral-specific inventory for anthropogenic Fe emissions (Rathod et al., 2020).

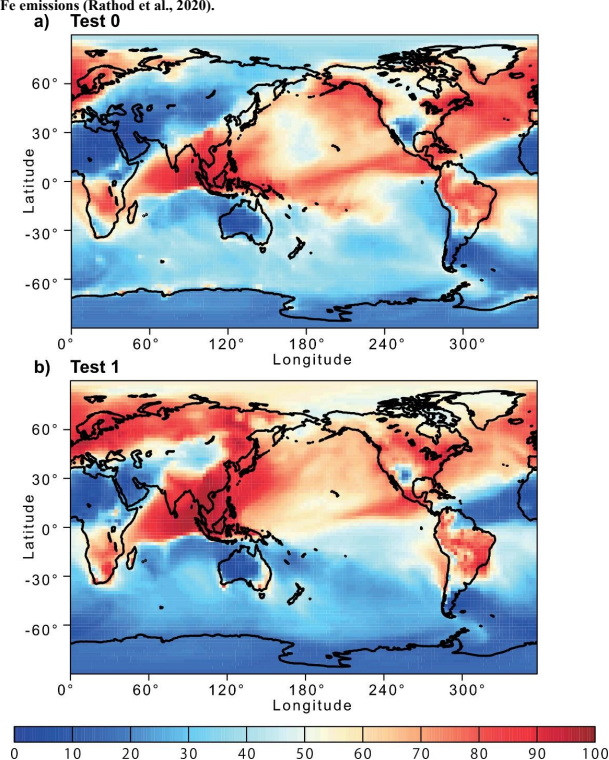


Figure 11: Proportion (%) of pyrogenic dissolved Fe in aerosol dissolved Fe concentration near the surface from a) Test 0 and b) Test 1 for December 2008 and January 2009. In Test 0, we ran the model without upgrades in the Fe dissolution scheme (Ito et al., 2021a) and applying the proton-promoted, oxalate-promoted and photoinduced dissolution schemes for combustion aerosols Table S3 (Ito, 2015). The proton + oxalate dissolution scheme (Table 1) was applied in Test 1 and we adopted the mineral-specific inventory for anthropogenic Fe emissions (Rathod et al., 2020).

Commented [MP71]: Is that only the anthropogenic fraction of pyrogenic Fe? Maybe stick to CFA-Fe or anthropogenic-Fe if more accurate?

I would suggest to change the caption to 'Contribution of pyrogenic aerosols to the atmospheric dissolved Fe loading...'

Commented [MP72]: Maybe Figures 10 and 11 could go to SI as they are only very briefly discussed



References

- Baker, A. R., Li, M., and Chance, R.: Trace Metal Fractional Solubility in Size-Segregated Aerosols From the Tropical Eastern Atlantic Ocean, *Global Biogeochem.*, 34, e2019GB006510, doi: 10.1029/2019GB006510, 2020.
- Baker, A. R., Kanakidou, M., Nenes, A., Myriokefalitakis, S., Croot, P. L., Duce, R. A., Gao, Y., Guieu, C., Ito, A., Jickells, T. D., Mahowald, N. M., Middag, R., Perron, M. M. G., Sarin, M. M., Shelley, R., and Turner, D. R.: Changing atmospheric acidity as a modulator of nutrient deposition and ocean biogeochemistry, *Sci. Adv.*, 7, eabd8800, doi: 10.1126/sciadv.abd8800, 2021.
- Baldo, C., Formenti, P., Nowak, S., Chevaillier, S., Cazaunau, M., Pangui, E., Di Biagio, C., Doussin, J. F., Ignatyev, K., Dagsson-Waldhauserova, P., Arnalds, O., MacKenzie, A. R., and Shi, Z.: Distinct chemical and mineralogical composition of Icelandic dust compared to northern African and Asian dust, *Atmos. Chem. Phys.*, 20, 13521-13539, doi: 10.5194/acp-2013521-2020, 2020.
- Bibi, I., Singh, B., and Silvester, E.: Dissolution kinetics of soil clays in sulfuric acid solutions: Ionic strength and temperature effects, *Appl. Geochem.*, 51, 170-183, doi: 10.1016/j.apgeochem.2014.10.004, 2014.
- Bikkina, S., Kawamura, K., Sarin, M., and Tachibana, E.: ^{13}C Probing of Ambient Photo-Fenton Reactions Involving Iron and Oxalic Acid: Implications for Oceanic Biogeochemistry, *ACS Earth Space Chem.*, 4, 964-976, doi: 10.1021/acsearthspacechem.0c00063, 2020.
- Blissett, R. S., and Rowson, N. A.: A review of the multi-component utilisation of coal fly ash, *Fuel*, 97, 1-23, doi: 10.1016/j.fuel.2012.03.024, 2012.
- Borgatta, J., Paskavitz, A., Kim, D., and Navea, J. G.: Comparative evaluation of iron leach from different sources of fly ash under atmospherically relevant conditions, *Environ. Chem.*, 13, 902-912, doi: 10.1071/en16046, 2016.
- Boyd, P. W., Jickells, T., Law, C. S., Blain, S., Boyle, E. A., Buesseler, K. O., Coale, K. H., Cullen, J. J., de Baar, H. J. W., Follows, M., Harvey, M., Lancelot, C., Levasseur, M., Owens, N. P. J., Pollard, R., Rivkin, R. B., Sarmiento, J., Schoemann, V., Smetacek, V., Takeda, S., Tsuda, A., Turner, S., and Watson, A. J.: Mesoscale Iron Enrichment Experiments 1993-2005: Synthesis and Future Directions, *Science*, 315, 612-617, doi: 10.1126/science.1131669, 2007.
- British Petroleum (BP): Statistical Review of World Energy 2020, available at <https://www.bp.com/en/global/corporate/energy-economics/statistical-review-of-world-energy.html>, (last access: 10 April 2021), 2020.
- Brown, P., Jones, T., and Bérubé, K.: The internal microstructure and fibrous mineralogy of fly ash from coal-burning power stations, *Environ. Pollut.*, 159, 3324-3333, doi: 10.1016/j.envpol.2011.08.041, 2011.



- Chen, H., Laskin, A., Baltrusaitis, J., Gorski, C. A., Scherer, M. M., and Grassian, V. H.: Coal fly ash as a source of iron in atmospheric dust, *Environ. Sci. Technol.*, 46, 2112-2120, doi: 10.1021/es204102f, 2012.
- Chen, H. H., and Grassian, V. H.: Iron Dissolution of Dust Source Materials during Simulated Acidic Processing: The Effect of Sulfuric, Acetic, and Oxalic Acids, *Environ. Sci. Technol.*, 47, 10312-10321, doi: 10.1021/es401285s, 2013.
- Cornell, R. M., Posner, A. M., and Quirk, J. P.: Kinetics and mechanisms of the acid dissolution of goethite (α -FeOOH), *Journal of Inorganic and Nuclear Chemistry*, 38, 563-567, doi: 10.1016/0022-1902(76)80305-3, 1976.
- Cornell, R. M., and Schwertmann, U.: *The Iron Oxides: Structure, Properties, Reactions, Occurrence and Uses*, Wiley-VCH, New York 2003.
- Cwiertny, D. M., Baltrusaitis, J., Hunter, G. J., Laskin, A., Scherer, M. M., and Grassian, V. H.: Characterization and acidmobilization study of iron-containing mineral dust source materials, *J. Geophys. Res.-Atmos.*, 113, D05202, doi: 10.1029/2007jd009332, 2008.
- Dudas, M. J., and Warren, C. J.: Submicroscopic model of fly ash particles, *Geoderma*, 40, 101-114, doi: 10.1016/00167061(87)90016-4, 1987.
- Eick, M. J., Peak, J. D., and Brady, W. D.: The Effect of Oxyanions on the Oxalate-Promoted Dissolution of Goethite, *SSSAJ*, 63, 1133-1141, doi: doi.org/10.2136/sssaj1999.6351133x, 1999.
- Emerson, E. W., Hodshire, A. L., DeBolt, H. M., Bilsback, K. R., Pierce, J. R., McMeeking, G. R., and Farmer, D. K.: Revisiting particle dry deposition and its role in radiative effect estimates, *PNAS USA*, 117, 26076-26082, doi: 10.1073/pnas.2014761117, 2020.
- Fu, H., Cwiertny, D. M., Carmichael, G. R., Scherer, M. M., and Grassian, V. H.: Photoreductive dissolution of Fe-containing mineral dust particles in acidic media, *Journal of Geophysical Research*, 115, D11304, doi: 10.1029/2009jd012702, 2010.
- Fu, H. B., Lin, J., Shang, G. F., Dong, W. B., Grassian, V. H., Carmichael, G. R., Li, Y., and Chen, J. M.: Solubility of Iron from Combustion Source Particles in Acidic Media Linked to Iron Speciation, *Environ. Sci. Technol.*, 46, 11119-11127, doi: 10.1021/es302558m, 2012.
- Furrer, G., and Stumm, W.: The coordination chemistry of weathering: I. Dissolution kinetics of δ -Al₂O₃ and BeO, *Geochim. Cosmochim. Ac.*, 50, 1847-1860, doi: 10.1016/0016-7037(86)90243-7, 1986.



- Hamer, M., Graham, R. C., Amrhein, C., and Bozhilov, K. N.: Dissolution of
ripidolite (Mg, Fe-chlorite) in organic and inorganic acid solutions, *SSSAJ*, 67, 654-
661, doi: 10.2136/sssaj2003.6540, 2003.
- Ito, A., and Feng, Y.: Role of dust alkalinity in acid mobilization of iron, *Atmos.*
Chem. Phys., 10, 9237-9250, doi:
10.5194/acp-10-9237-2010, 2010.
- Ito, A.: Atmospheric Processing of Combustion Aerosols as a Source of
Bioavailable Iron, *Environ. Sci. Technol. Lett.*, 2, 7075, doi:
10.1021/acs.estlett.5b00007, 2015.
- Ito, A., and Shi, Z.: Delivery of anthropogenic bioavailable iron from mineral dust
and combustion aerosols to the ocean, *Atmos. Chem. Phys.*, 16, 85-99, doi:
10.5194/acp-16-85-2016, 2016.
- Ito, A., Lin, G. X., and Penner, J. E.: Radiative forcing by light-absorbing aerosols
of pyrogenic iron oxides, *Sci. Rep.*, 8, 7347, doi: 10.1038/s41598-018-25756-3,
2018.
- Ito, A., Myriokefalitakis, S., Kanakidou, M., Mahowald, N. M., Scanza, R. A.,
Hamilton, D. S., Baker, A. R., Jickells, T.,
Sarin, M., Bikkina, S., Gao, Y., Shelley, R. U., Buck, C. S., Landing, W. M., Bowie,
A. R., Perron, M. M. G., Guieu, C., Meskhidze, N., Johnson, M. S., Feng, Y., Kok,
J. F., Nenes, A., and Duce, R. A.: Pyrogenic iron: The missing link to high iron
solubility in aerosols, *Sci. Adv.*, 5, eaau7671 doi: 10.1126/sciadv.aau7671, 2019.
- Ito, A., Adebisi, A. A., Huang, Y., and Kok, J. F.: Less atmospheric radiative
heating due to aspherical dust with coarser size, *Atmos. Chem. Phys. Discuss.*, 2021,
1-44, doi: 10.5194/acp-2021-134, 2021a.
- Ito, A., Ye, Y., Baldo, C., and Shi, Z.: Ocean fertilization by pyrogenic aerosol iron,
npj Clim. Atmos. Sci., 4, 30, doi:
10.1038/s41612-021-00185-8, 2021b.
- Jickells, T., and Moore, C. M.: The importance of Atmospheric Deposition for
Ocean Productivity, *Annu. Rev. Ecol. Evol. Syst.*, 46, 481-501, doi:
10.1146/annurev-ecolsys-112414-054118, 2015.
- Jickells, T. D., An, Z. S., Andersen, K. K., Baker, A. R., Bergametti, G., Brooks, N.,
Cao, J. J., Boyd, P. W., Duce, R. A., Hunter, K. A., Kawahata, H., Kubilay, N.,
laRoche, J., Liss, P. S., Mahowald, N., Prospero, J. M., Ridgwell, A. J., Tegen, I.,
and Torres, R.: Global iron connections between desert dust, ocean
biogeochemistry, and climate, *Science*, 308, 67-71, doi:
10.1126/science.1105959, 2005.
- Jones, D. R.: The Leaching of Major and Trace Elements from Coal Ash, in:
Environmental Aspects of Trace Elements in Coal, edited by: Swaine, D. J., and
Goodarzi, F., Springer Netherlands, Dordrecht, 221-262, 1995.
- Kanakidou, M., Myriokefalitakis, S., and Tsigaridis, K.: Aerosols in atmospheric
chemistry and biogeochemical cycles of nutrients, *Environ. Res. Lett.*, 13, 063004,
doi: 10.1088/1748-9326/aabddb, 2018.



- 771 Kawamura, K., and Bikkina, S.: A review of dicarboxylic acids and related
772 compounds in atmospheric aerosols: Molecular distributions, sources and
773 transformation, *Atmos. Res.*, 170, 140-160, doi: 10.1016/j.atmosres.2015.11.018,
774 2016.
- 775 Kim, D., Xiao, Y., Karchere-Sun, R., Richmond, E., Ricker, H. M., Leonardi, A.,
776 and Navea, J. G.: Atmospheric Processing of Anthropogenic Combustion Particles:
777 Effects of Acid Media and Solar Flux on the Iron Mobility from Fly Ash, *ACS Earth*
778 *Space Chem.*, 4, 750-761, doi: 10.1021/acsearthspacechem.0c00057, 2020.
- 779 Kukier, U., Ishak, C. F., Sumner, M. E., and Miller, W. P.: Composition and
780 element solubility of magnetic and non-magnetic fly ash fractions, *Environ. Pollut.*,
781 123, 255-266, doi: 10.1016/S0269-7491(02)00376-7, 2003.
- 782 Kumar, A., Sarin, M. M., and Srinivas, B.: Aerosol iron solubility over Bay of
783 Bengal: Role of anthropogenic sources and chemical processing, *Mar. Chem.*, 121,
784 167-175, doi: 10.1016/j.marchem.2010.04.005, 2010.
- 785 Kutchko, B. G., and Kim, A. G.: Fly ash characterization by SEM-EDS, *Fuel*, 85,
786 2537-2544, doi: 10.1016/j.fuel.2006.05.016, 2006.
- 787 Lawson, M. J., Prytherch, Z. C., Jones, T. P., Adams, R. A., and Bérubé, K. A.:
788 Iron-Rich Magnetic Coal Fly Ash Particles Induce Apoptosis in Human Bronchial
789 Cells, *Appl. Sci.*, 10, 8368, doi: 10.3390/app10238368, 2020.
- 790 Lee, S. O., Tran, T., Jung, B. H., Kim, S. J., and Kim, M. J.: Dissolution of iron
791 oxide using oxalic acid, *Hydrometallurgy*, 87, 91-99, doi:
792 10.1016/j.hydromet.2007.02.005, 2007.
- 793 Li, J., Anderson, J. R., and Buseck, P. R.: TEM study of aerosol particles from clean
794 and polluted marine boundary layers over the North Atlantic, *J. Geophys. Res.-*
795 *Atmos.*, 108, doi: 10.1029/2002JD002106, 2003.
- 796 Li, W. J., Xu, L., Liu, X. H., Zhang, J. C., Lin, Y. T., Yao, X. H., Gao, H. W.,
797 Zhang, D. Z., Chen, J. M., Wang, W. X., Harrison, R. M., Zhang, X. Y., Shao, L. Y.,
798 Fu, P. Q., Nenes, A., and Shi, Z. B.: Air pollution-aerosol interactions produce more
799 bioavailable iron for ocean ecosystems, *Sci. Adv.*, 3, e1601749, doi:
800 10.1126/sciadv.1601749, 2017.
- 801 Mahowald, N. M., Kloster, S., Engelstaedter, S., Moore, J. K., Mukhopadhyay, S.,
802 McConnell, J. R., Albani, S., Doney, S. C., Bhattacharya, A., Curran, M. A. J.,
803 Flanner, M. G., Hoffman, F. M., Lawrence, D. M., Lindsay, K., Mayewski, P. A.,
804 Neff, J., Rothenberg, D., Thomas, E., Thornton, P. E., and Zender, C. S.: Observed
805 20th century desert dust variability: impact on climate and biogeochemistry, *Atmos.*
806 *Chem. Phys.*, 10, 10875-10893, doi: 10.5194/acp-10-10875-2010, 2010.



- Marcotte, A. R., Anbar, A. D., Majestic, B. J., and Herckes, P.: Mineral Dust and Iron Solubility: Effects of Composition, Particle Size, and Surface Area, *Atmosphere*, 11, 533, doi: 10.3390/atmos11050533, 2020.
- Martin, J. H.: Glacial-interglacial CO₂ change: The Iron Hypothesis, *Paleoceanography*, 5, 1-13, doi: 10.1029/PA005i001p00001, 1990.
- Matsuo, M., Kobayashi, T., Singh, T. B., Tsurumi, M., and Ichikuni, M.: ⁵⁷Fe Mössbauer spectroscopic study of Japanese cedar bark — The variation in chemical states of iron due to influence of human activities, *Hyperfine Interact.*, 71, 1255-1258, doi: 10.1007/BF02397311, 1992.
- Meskhidze, N., Chameides, W. L., Nenes, A., and Chen, G.: Iron mobilization in mineral dust: Can anthropogenic SO₂ emissions affect ocean productivity?, *Geophys. Res. Lett.*, 30, 2085, doi: 10.1029/2003gl018035, 2003.
- Mills, M. M., Ridame, C., Davey, M., La Roche, J., and Geider, R. J.: Iron and phosphorus co-limit nitrogen fixation in the eastern tropical North Atlantic, *Nature*, 429, 292-294, doi: 10.1038/nature02550, 2004.
- Moore, C. M., Mills, M. M., Milne, A., Langlois, R., Achterberg, E. P., Lochte, K., Geider, R. J., and La Roche, J.: Iron limits primary productivity during spring bloom development in the central North Atlantic, *Glob. Change Biol.*, 12, 626-634, doi: 10.1111/j.1365-2486.2006.01122.x, 2006.
- Munawer, M. E.: Human health and environmental impacts of coal combustion and post-combustion wastes, *J. Sustain. Min.*, 17, 87-96, doi: 10.1016/j.jsm.2017.12.007, 2018.
- Myriokefalitakis, S., Ito, A., Kanakidou, M., Nenes, A., Krol, M. C., Mahowald, N. M., Scanza, R. A., Hamilton, D. S., Johnson, M. S., Meskhidze, N., Kok, J. F., Guieu, C., Baker, A. R., Jickells, T. D., Sarin, M. M., Bikkina, S., Shelley, R., Bowie, A., Perron, M. M. G., and Duce, R. A.: Reviews and syntheses: the GESAMP atmospheric iron deposition model intercomparison study, *Biogeosciences*, 15, 6659-6684, doi: 10.5194/bg-15-6659-2018, 2018.
- Paris, R., Desboeufs, K. V., and Journet, E.: Variability of dust iron solubility in atmospheric waters: Investigation of the role of oxalate organic complexation, *Atmos. Environ.*, 45, 6510-6517, doi: 10.1016/j.atmosenv.2011.08.068, 2011.
- Paris, R., and Desboeufs, K. V.: Effect of atmospheric organic complexation on iron-bearing dust solubility, *Atmos. Chem. Phys.*, 13, 4895-4905, doi: 10.5194/acp-13-4895-2013, 2013.
- Poulton, S. W., and Canfield, D. E.: Development of a sequential extraction procedure for iron: implications for iron partitioning in continentally derived particulates, *Chem. Geol.*, 214, 209-221, doi: 10.1016/j.chemgeo.2004.09.003, 2005.
- Pye, H. O. T., Nenes, A., Alexander, B., Ault, A. P., Barth, M. C., Clegg, S. L., Collett Jr, J. L., Fahey, K. M., Hennigan, C. J., Herrmann, H., Kanakidou, M., Kelly,



- 848 J. T., Ku, I. T., McNeill, V. F., Riemer, N., Schaefer, T., Shi, G., Tilgner, A.,
849 Walker,
850 J. T., Wang, T., Weber, R., Xing, J., Zaveri, R. A., and Zuend, A.: The acidity of
851 atmospheric particles and clouds, *Atmos. Chem. Phys.*, 20, 4809–4888, doi:
852 10.5194/acp-20-4809-2020, 2020.
853 Raiswell, R., Benning, L. G., Tranter, M., and Tulaczyk, S.: Bioavailable iron in the
854 Southern Ocean: the significance of the iceberg conveyor belt, *Geochemical*
855 *Transactions*, 9, doi: 10.1186/1467-4866-9-7, 2008.
856 Rathod, S. D., Hamilton, D. S., Mahowald, N. M., Klimont, Z., Corbett, J. J., and
857 Bond, T. C.: A Mineralogy-Based Anthropogenic Combustion - Iron Emission
858 Inventory, *J. Geophys. Res.-Atmos*, 125, e2019JD032114, doi:
859 10.1029/2019jd032114, 2020.
860 Ravel, B., and Newville, M.: ATHENA, ARTEMIS, HEPHAESTUS: data analysis
861 for X-ray absorption spectroscopy using IFEFFIT, *J. Synchrotron Radiat.*, 12, 537–
862 541, doi: 10.1107/S0909049505012719, 2005.
863 Rubasinghege, G., Lentz, R. W., Scherer, M. M., and Grassian, V. H.: Simulated
864 atmospheric processing of iron oxyhydroxide minerals at low pH: roles of particle
865 size and acid anion in iron dissolution, *PNAS USA*, 107, 6628–6633, doi:
866 10.1073/pnas.0910809107, 2010.
867 Rubin, M., Berman-Frank, I., and Shaked, Y.: Dust- and mineral-iron utilization by
868 the marine dinitrogen-fixer *Trichodesmium*, *Nat. Geosci.*, 4, 529–534, doi:
869 10.1038/ngeo1181, 2011.
870 Schlosser, C., Schmidt, K., Aquilina, A., Homoky, W. B., Castrillejo, M., Mills, R.
871 A., Patey, M. D., Fielding, S., Atkinson, A., and Achterberg, E. P.: Mechanisms of
872 dissolved and labile particulate iron supply to shelf waters and phytoplankton
873 blooms off South Georgia, Southern Ocean, *Biogeosciences*, 15, 4973–4993, doi:
874 10.5194/bg-15-4973-2018, 2018.
875 Schroth, A. W., Crusius, J., Sholkovitz, E. R., and Bostick, B. C.: Iron solubility
876 driven by speciation in dust sources to the ocean, *Nat. Geosci.*, 2, 337–340, doi:
877 10.1038/ngeo501, 2009.
878 Schwertmann, U.: Solubility and dissolution of iron oxides, *Plant Soil*, 130, 1–25,
879 doi: 10.1007/BF00011851, 1991.
880 Seinfeld, J. H., and Pandis, S. N.: *Atmospheric chemistry and physics: from air*
881 *pollution to climate change*, John Wiley & Sons, 2016.
882 Shi, Z., Krom, M. D., Bonneville, S., Baker, A. R., Jickells, T. D., and Benning, L.
883 G.: Formation of iron nanoparticles and increase in iron reactivity in the mineral



dust during simulated cloud processing, *Environ. Sci. Technol.*, 43, 6592-6596, doi:
10.1021/es901294g, 2009.

Shi, Z., Bonneville, S., Krom, M. D., Carslaw, K. S., Jickells, T. D., Baker, A. R.,
and Benning, L. G.: Iron dissolution kinetics of mineral dust at low pH during
simulated atmospheric processing, *Atmos. Chem. Phys.*, 11, 995-1007, doi:
10.5194/acp-11995-2011, 2011a.

Shi, Z., Krom, M. D., Bonneville, S., Baker, A. R., Bristow, C., Drake, N., Mann,
G., Carslaw, K., McQuaid, J. B., Jickells, T., and Benning, L. G.: Influence of
chemical weathering and aging of iron oxides on the potential iron solubility of
Saharan dust during simulated atmospheric processing, *Global Biogeochem.*, 25,
GB2010, doi: 10.1029/2010gb003837, 2011b.

Shi, Z., Krom, M. D., Jickells, T. D., Bonneville, S., Carslaw, K. S., Mihalopoulos,
N., Baker, A. R., and Benning, L. G.:
Impacts on iron solubility in the mineral dust by processes in the source region and
the atmosphere: A review, *Aeolian Res.*, 5, 21-42, doi:
10.1016/j.aeolia.2012.03.001, 2012.

Shi, Z., Krom, M. D., Bonneville, S., and Benning, L. G.: Atmospheric processing
outside clouds increases soluble iron in mineral dust, *Environ. Sci. Technol.*, 49,
1472-1477, doi: 10.1021/es504623x, 2015.

Shi, Z. B., Woodhouse, M. T., Carslaw, K. S., Krom, M. D., Mann, G. W., Baker,
A. R., Savov, I., Fones, G. R., Brooks, B., Drake, N., Jickells, T. D., and Benning,
L. G.: Minor effect of physical size sorting on iron solubility of transported mineral
dust, *Atmos. Chem. Phys.*, 11, 8459-8469, doi: 10.5194/acp-11-8459-2011, 2011c.

Sidhu, P. S., Gilkes, R. J., Cornell, R. M., Posner, A. M., and Quirk, J. P.:
Dissolution of Iron Oxides and Oxyhydroxides in Hydrochloric and Perchloric
Acids, *Clays Clay Miner.*, 29, 269-276, doi: 10.1346/CCMN.1981.0290404, 1981.

Spokes, L. J., and Jickells, T. D.: Factors controlling the solubility of aerosol trace
metals in the atmosphere and on mixing into seawater, *Aquat. Geochem.*, 1, 355-
374, doi: 10.1007/BF00702739, 1995.

Srinivas, B., Sarin, M. M., and Kumar, A.: Impact of anthropogenic sources on
aerosol iron solubility over the Bay of Bengal and the Arabian Sea,
Biogeochemistry, 110, 257-268, doi: 10.1007/s10533-011-9680-1, 2012.

Srinivas, B., and Sarin, M. M.: Atmospheric dry-deposition of mineral dust and
anthropogenic trace metals to the Bay of Bengal, *J. Mar. Syst.*, 126, 56-68, doi:
10.1016/j.jmarsys.2012.11.004, 2013.

Surana, V., and Warren, I.: The leaching of goethite, *Transactions of the Institute of
Mining and Metallurgy*, 80, C152-155, 1969.

Sutto, T. E.: Magnetite fine particle and nanoparticle environmental contamination
from industrial uses of coal, *Environ. Pollut.*, 243, 528-533, doi:
10.1016/j.envpol.2018.08.080, 2018.



- 924 Valeev, D., Mikhailova, A., and Atmadzhidi, A.: Kinetics of Iron Extraction from
925 Coal Fly Ash by Hydrochloric Acid Leaching, *Metals*, 8, 533, doi:
926 10.3390/met8070533, 2018.
- 927 Valeev, D., Kunilova, I., Alpatov, A., Varnavskaya, A., and Ju, D.: Magnetite and
928 Carbon Extraction from Coal Fly Ash Using Magnetic Separation and Flotation
929 Methods, *Minerals*, 9, 320, doi: 10.3390/min9050320, 2019.
- 930 Viollier, E., Inglett, P. W., Hunter, K., Roychoudhury, A. N., and Van Cappellen, P.:
931 The ferrozine method revisited: Fe(II)/Fe(III) determination in natural waters, *Appl.*
932 *Geochem.*, 15, 785-790, doi: 10.1016/s0883-2927(99)00097-9, 2000.
- 933 Waanders, F. B., Vinken, E., Mans, A., and Mulaba-Bafubandi, A. F.: Iron
934 Minerals in Coal, Weathered Coal and Coal Ash – SEM and Mössbauer Results,
935 *Hyperfine Interact.*, 148, 21-29, doi: 10.1023/B:HYPE.0000003760.89706.f6, 2003.
- 936 Wang, R., Balkanski, Y., Boucher, O., Bopp, L., Chappell, A., Ciais, P.,
937 Hauglustaine, D., Penuelas, J., and Tao, S.: Sources, transport and deposition of iron
938 in the global atmosphere, *Atmos. Chem. Phys.*, 15, 6247-6270, doi: 10.5194/acp-15-
939 62472015, 2015.
- 940 Wang, X. S.: Mineralogical and chemical composition of magnetic fly ash fraction,
941 *Environ. Earth Sci.*, 71, 1673-1681, doi:
942 10.1007/s12665-013-2571-0, 2014.
- 943 Warren, C. J., and Dudas, M. J.: Leachability and partitioning of elements in
944 ferromagnetic fly ash particles, *Sci. Total Environ.*, 84, 223-236, doi: 10.1016/0048-
945 9697(89)90385-9, 1989.
- 946 Wexler, A. S., and Clegg, S. L.: Atmospheric aerosol models for systems including
947 the ions H^+ , NH_4^+ , Na^+ , SO_4^{2-} , NO_3^- , Cl^- , Br^- , and H_2O , *J. Geophys. Res.-Atmos.*,
948 107, 4207, doi: 10.1029/2001JD000451, 2002.
- 949 Xu, N., and Gao, Y.: Characterization of hematite dissolution affected by oxalate
950 coating, kinetics and pH, *Appl. Geochem.*, 23, 783-793, doi:
951 10.1016/j.apgeochem.2007.12.026, 2008.
- 952 Yao, Z. T., Ji, X. S., Sarker, P. K., Tang, J. H., Ge, L. Q., Xia, M. S., and Xi, Y. Q.:
953 A comprehensive review on the applications of coal fly ash, *Earth-Sci. Rev.*, 141,
954 105-121, doi: 10.1016/j.earscirev.2014.11.016, 2015.
- 955 Yu, J. Z., Huang, X.-F., Xu, J., and Hu, M.: When Aerosol Sulfate Goes Up, So
956 Does Oxalate: Implication for the Formation Mechanisms of Oxalate, *Environ. Sci.*
957 *Technol.*, 39, 128-133, doi: 10.1021/es049559f, 2005.
- 958 Zhang, D., Iwasaka, Y., Shi, G., Zang, J., Matsuki, A., and Trochkin, D.: Mixture
959 state and size of Asian dust particles collected at southwestern Japan in spring 2000,
960 *J. Geophys. Res.-Atmos.*, 108, 4760, doi: 10.1029/2003JD003869, 2003.

<https://doi.org/10.5194/acp-2021-748>

Preprint. Discussion started: 30 September 2021

© Author(s) 2021. CC BY 4.0 License.



Atmospheric
Chemistry
and Physics
Discussions



961 Zhao, Y., Zhang, J., Sun, J., Bai, X., and Zheng, C.: Mineralogy, Chemical
962 Composition, and Microstructure of Ferrospheres in Fly Ashes from Coal
963 Combustion, *Energy Fuels*, 20, 1490-1497, doi: 10.1021/ef060008f, 2006.
964 Zhu, X. R., Prospero, J. M., Millero, F. J., Savoie, D. L., and Brass, G. W.: The
965 solubility of ferric ion in marine mineral aerosol solutions at ambient relative
966 humidities *Mar. Chem.*, 38, 91-107, doi: 10.1016/0304-4203(92)90069-m, 1992.
967